Probing environment fluctuations by two-dimensional electronic spectroscopy of molecular systems at temperatures below 5 K

Olga Rancova, Ryszard Jankowiak, and Darius Abramavicius

Articles you may be interested in

Measuring correlated electronic and vibrational spectral dynamics using line shapes in two-dimensional electronic-vibrational spectroscopy
J. Chem. Phys. **142**, 174202 (2015); 10.1063/1.4919686

Determining the static electronic and vibrational energy correlations via two-dimensional electronic-vibrational spectroscopy
J. Chem. Phys. **142**, 174201 (2015); 10.1063/1.4919684

Accidental vibrational degeneracy in vibrational excited states observed with ultrafast two-dimensional IR vibrational echo spectroscopy
J. Chem. Phys. **123**, 164301 (2005); 10.1063/1.2071967

Heterodyned fifth-order two-dimensional IR spectroscopy: Third-quantum states and polarization selectivity
J. Chem. Phys. **123**, 094502 (2005); 10.1063/1.1998829

State-to-state unimolecular reaction dynamics of HOCl near the dissociation threshold: The role of vibrations, rotations, and IVR probed by time- and eigenstate-resolved spectroscopy
J. Chem. Phys. **111**, 7359 (1999); 10.1063/1.480058

Probing environment fluctuations by two-dimensional electronic spectroscopy of molecular systems at temperatures below 5 K

Olga Rancova,[1] Ryszard Jankowiak,[2] and Darius Abramavicius[1]

[1]*Department of Theoretical Physics, Vilnius University, Sauletekio al 9-III, 10222 Vilnius, Lithuania*

[2]*Department of Chemistry and Department of Physics, Kansas State University, 213 CBC Building Manhattan, Kansas 66506-0401, USA*

Two-dimensional (2D) electronic spectroscopy at cryogenic and room temperatures reveals excitation energy relaxation and transport, as well as vibrational dynamics, in molecular systems. These phenomena are related to the spectral densities of nuclear degrees of freedom, which are directly accessible by means of hole burning and fluorescence line narrowing approaches at low temperatures (few K). The 2D spectroscopy, in principle, should reveal more details about the fluctuating environment than the 1D approaches due to peak extension into extra dimension. By studying the spectral line shapes of a dimeric aggregate at low temperature, we demonstrate that 2D spectra have the potential to reveal the fluctuation spectral densities for different electronic states, the interstate correlation of static disorder and, finally, the time scales of spectral diffusion with high resolution. © *2015 AIP Publishing LLC.* [http://dx.doi.org/10.1063/1.4918584]

NOMENCLATURE

2DES	Two-dimensional electronic spectroscopy
HB	Hole burning
FLN	Fluorescence line narrowing
ΔFLN:	Difference FLN
ZPL	Zero phonon line
EET	Excitation energy transfer
DOF	Degrees of freedom
ESE	Excited state emission
GSB	Ground state bleach
ESA	Excited state absorption
WSCP	Water-soluble chlorophyll protein
LvWSCP	WSCP from Lepidium virginicum
CaWSCP	WSCP from cauliflower (Brassica oleracea L. var. botrys)
LO	Local oscillator
RP	Rephasing
NRP	Non-rephasing
PP	Pump-probe
PHB	Photochemical HB
NPHB	Non-photochemical HB
CP	Charge-pair
ZPH	Zero-phonon hole
PSB	Phonon side band
HR	Huang-Rhys
LA	Linear absorption
ZPP	Zero-phonon-peak

I. INTRODUCTION

During the last 10 yr, a two-dimensional electronic spectroscopy (2DES) has become a routine tool to study non-equilibrium short time dynamics of synthetic and biological molecular aggregates.[1–12] Probably, the milestone advancement of the technique was direct demonstration of electronic and vibrational, as well as mixed, quantum coherences via femtosecond beats of various diagonal and off-diagonal peaks in the 2D plots from 77 K up to room temperature.[1,5,7,13–18] These results attained much interest and caused intensive debates on the origin and functional purpose of the oscillations: whether they arise from quantum excitation dynamics in bio-materials purposefully optimized by nature, or the oscillations record merely bond wiggling, which is natural and not necessarily a quantum phenomenon.[5,7,16,19–26] However, it has been acknowledged that nuclear dynamics and its coupling to the electronic excitations leads to the important physical dynamic processes leading to energy photoconversion.[21,26–29] Thus, the most important questions are what is the cumulative nuclear response to the electronic excitations and whether there is a feedback.

In terminology of open quantum systems, the electronic degrees of freedom are associated with the observable quantum system of interest and all nuclear degrees of freedom (DOF) stand for the bath, characterized by the spectral density. The latter is represented by a continuous function. Its smooth background results from the so-called *phonon* modes and causes spectral broadening and relaxation, while the sharp peaks in it reflect couplings between the quantum system and the specific coherent molecular vibrations. The *vibrational* beats in the 2D spectra thus reflect specific resonances of the bath spectral density.[24,25,30]

The spectral density is often obtained from low temperature (few K) measurements, where the spectral density function becomes clearly imprinted onto the spectral line shapes.[31] Techniques like hole burning (HB), fluorescence line narrowing (FLN), and difference FLN (ΔFLN) reveal the properties of nuclear vibrations with high resolution and directly indicate the possible electronic-vibrational coupling

142, 212428-1

patterns that appear outside the so-called zero phonon line (ZPL) which signifies the electronic-only transition, when vibrational quanta are conserved. Application of such approaches to specific photosynthetic aggregates revealed the spectral density for a range of significant photosynthetic systems.[32–38] We note that HB spectroscopy (via zero-phonon action spectra, i.e., burning of resonant holes at the lowest energy state using constant fluence) can also provide information about static (inhomogeneous) broadening, while the width of resonant holes (burned at various spectral regions) can reveal information on excitation energy transfer (EET) and charge-transfer processes in model and complex biological systems. It should be noted that the few K temperature also allows following of the photosynthesis-relevant processes, since basic light harvesting, excitation transport and charge separation still take place in these conditions. Consequently, the systems are still intact and important functional mechanisms can be revealed without interference of the inhomogeneous broadening.

It follows that the same information on the nuclear degrees of freedom is encoded in the beats and decays of the time resolved 2DES, as well as in high-resolution spectral line shapes. The extra dimension in 2DES allows to dissect distinct electron-vibrational couplings related to the specific electronic transitions by tracking different peaks. This selection becomes available by tuning lasers to specific electronic resonances and by tracking down distinct interaction patterns: excited state emission (ESE), ground state bleach (GSB), and excited state absorption (ESA).[4,39] It has been recently shown that spectral beats at different frequencies can be sorted out by making so-called frequency maps.[5,7,18,23] However, the same information should be available from the high resolution spectral line shapes taken along the two ω_1 and ω_3 frequency axes, where ω_1 represents the excitation frequency while ω_3 reflects detection frequency.

In spectroscopic measurements, the nuclear DOF are additionally sorted out into static and dynamic ones. These cause the inhomogeneous and homogeneous broadening of the spectral lines, respectively. The spectral density is associated with the dynamic fluctuations while static ones become eliminated by HB at low temperatures.[31] One of the many merits of 2D spectra is that it resolves homogeneous and inhomogeneous linewidths in different directions in the so-called rephasing signal.[6,40] However the other, non-rephasing, contribution strongly interferes the signal at ambient temperature making complete extraction of the rephasing part practically impossible.

In this paper, we present numerical simulations of 2DES spectra of a homodimer model (two coupled pigments of the same kind) at low temperature and relate characteristics of the fluctuating environment and the spectral line shapes. The chosen system is simple enough so that obtained spectral responses can be easily related to the particular characteristics of the system, while it is sufficiently complicated so that excitation delocalization and fluctuation correlation effects are observed. The parameters of our model are inspired by the HB and FLN spectroscopies of a recombinant water-soluble chlorophyll protein (WSCP).[36,37,41]

It has been shown recently that both WSCP from Lepidium virginicum (LvWSCP) and cauliflower (Brassica oleracea L. var. botrys - CaWSCP) have four chlorophylls in a tetramer, i.e., two weakly coupled dimers[42] in which uncorrelated EET was observed.[73] Additionally, its 2DES spectra at 77 K showed vibrational beats.[43] Phonon spectral density of this system has been experimentally determined[36,37,44] and is used here to study a model dimer. Experimental and theoretical HB and 2DES data of the recombinant tetramer LvWSCP and CaWSCP will be reported elsewhere.

In this work, we study the high-resolution spectral profiles along the ω_1 and ω_3 axes as well as 2D features of the ZPL in the 2DES spectra and demonstrate that the spectral density, related to different excitonic states, can be directly accessed. Additionally, at few K temperature, the non-rephasing part is much weaker than the rephasing and the static disorder becomes clearly resolved. The 2D shapes of the ZPL then reveal correlation characteristics of the disorder between different electronic states. In this context, the combination of 2DES and low temperature provides the information on the electronic coupling to nuclear fluctuations (dynamic and static) with great level of detail. Surprisingly, to our knowledge, there are still neither experimental nor theoretical data published on the low temperature 2DES.

The paper is organized as follows. In Sec. II, we describe in general the method of 2DES and traditional low temperature approaches, i.e., various types of HB, FLN. In Sec. III, we consider the contributions to the 2DES spectra in the case of thermalized excitation (long t_2 delay). This case is shown to better reflect properties of traditional HB. Next, we study 2D spectral shapes of 2DES. Section IV is devoted to a single chromophore, while Sec. V considers a dimer model. In Sec. VI, we describe the complexity of the system and its fluctuations, which has been shown to strongly affect the 2DES spectra. Again, the 2DES and HB are related to each other in this section and their differences are highlighted. The Conclusions (Sec. VII) summarizes the findings.

II. TWO DIMENSIONAL ELECTRONIC SPECTROSCOPY AND RELEVANT LOW-T TECHNIQUES

2DES is a specific representation of the four-wave-mixing signal. In terms of the perturbation theory, it is given by the third order optical response function, which relates the polarization of the excitonic system to the incoming chronologically ordered optical fields.[4,28,45,55] Depending on the configuration of the wave vectors of the incident pulses and the local oscillator (LO) fields, the signal of the polarization-induced optical field can be detected in rephasing (RP) and non-rephasing (NRP) interaction configurations with resulting field wave vectors: $k_{RP} = -k_1 + k_2 + k_3$ and $k_{NRP} = +k_1 - k_2 + k_3$; where k_i are the wave vectors of the incident fields. The sum of RP and NRP configurations results in pump-probe (PP)-like response, which is sometimes denoted as the total signal. In practice, however, the PP is always measured, and additional assumptions are necessary to reveal the RP and NRP parts.

Delay time between the first and second incident pulses, t_1, and the third and LO pulses, t_3, are Fourier transformed to give the frequency grid (ω_1, ω_3) for the 2D spectra; here,

ω_1 corresponds to the excitation and ω_3 to the detection frequencies. The delay time between the second and the third pulses t_2 tracks low and zero frequency dynamics (intraband coherences and populations, respectively) and it remains the parameter of the particular 2D spectrum. Hence, we denote the RP signal as $S_I(\omega_3, t_2, \omega_1)$ with negative ω_1, NRP as $S_{II}(\omega_3, t_2, \omega_1)$ with positive ω_1, and PP with positive ω_1 is given by

$$S_\Sigma(\omega_3, t_2, \omega_1) = S_I(\omega_3, t_2, -\omega_1) + S_{II}(\omega_3, t_2, \omega_1). \quad (1)$$

System-bath interactions broaden the spectral lines along both ω_1 and ω_3 axes. During the t_2 delay time, population transport (relaxation) and dephasing processes are taking place in the system as well. They are observed as t_2-dependent spectral features.[2,3,8,14,46–49] Two limiting cases are distinguished in this paper—the zero and infinite delay times. Of course, these are theoretical constructs of the model used in the simulations, where the number of electronic excitations never decay. For the realistic systems, the infinity should be understood with respect to the thermalization and intraband relaxation times. The electronic intraband relaxation occurs in picoseconds, on the same time scale as bath thermalization, while the electronic excitation decays within nanoseconds. Thus, infinity then denotes the time of a few hundred picoseconds between these limits when the electronic population has reached the lowest energy electronic state, and the bath has relaxed (thermalized) accordingly. However, at zero t_2 delay time, the electronic relaxation has not yet occurred after the excitation by two initial pulses; thus, the corresponding 2DES plot can be denoted by the electronic correlation plot.[6]

At low temperatures, there are several closely related spectroscopic measurements. The HB experiment is essentially the difference of the absorbance of the sample before and after "burning" by a narrow-band (less than a wavenumber bandwidth) laser.[31,50] At low temperatures, the conformational dynamics of the solvent is restricted, so the burning process takes a subset of members of the ensemble under consideration (either molecules or their complexes) out of equilibrium. That is, the HB technique relies on differences observed in the absorption spectrum of a low-temperature system after narrow-band laser excitation. If a pigment molecule (in resonance with the laser) experiences photochemical reaction, it ceases to absorb at its original wavelength/frequency and one speaks of photochemical HB (PHB). In the case of non-photochemical HB (NPHB), the pigment molecule does not undergo a chemical reaction, but its immediate environment experiences some rearrangement (for details, see Refs. 31 and 50). Both PHB and NPHB result in the formation of persistent holes, meaning the holes are preserved after the initial excitation is turned off, as long as low temperature is maintained. In either cases, the HB spectrum is obtained as the difference between the measured absorption spectrum before and after laser excitation.

In the case of transient HB spectra, the difference absorption spectrum decays when the burn laser is switched off, i.e., together with the decay of electronic excitation. Usually, the presence of a different relatively long-lived (bottleneck) state is assumed. For example, the excited state

can evolve into a triplet state or is converted photochemically to another long-lived (μs to ms range) product (e.g., a charge-pair (CP) state), leaving a transient hole in the absorption spectrum with a zero-phonon hole (ZPH) at the frequency of the original excitation (resonant HB) and with shape defined by the strength of electron-phonon coupling. In this case, the pigment's ground state is depopulated for the lifetime of the long-lived state and the spectral hole will be observable only for the duration of this lifetime. However, the electronic excitations in photosynthetic aggregates have a natural lifetime of ns, and the electronically excited pigment cannot absorb a second photon at the same frequency. The pigment will show bleach signal and absorption at different frequency in the same meaning as in pump-probe spectroscopy. Hence, the triplet or CP states in principle are not necessary for the transient absorption changes measured in the time-domain (i.e., using pulsed instead of CW lasers typically employed in HB spectroscopy).

Thus, in either cases of HB, the absorbance after the burn process lacks that subset of the absorbers (depleted from the ground state) leading to the observed bleach, i.e., HB spectra. Since the bleached absorbers reside in somewhat different configuration, burning may lead to induced emission and additional absorption (anti-holes) in other spectral regions in the HB spectrum.

The use of low temperatures and narrow-band excitation becomes natural when taking into account that the homogeneous linewidths are of the order of few wavenumbers, and the ZPL becomes resolved. Additional side-peaks involve creation (emission) of one or several vibrational quanta. For the continuous bath spectral density, this causes the so-called phonon side band (PSB) away from the ZPL. The shape of PSB approximately follows the spectral density $J(\omega)$, which describes the distribution of Huang-Rhys (HR) parameter s_h with frequency. For the details, the reader is referred to Refs. 31 and 50–53.

The FLN experiment is somewhat similar; however, instead of absorbance, the spontaneous emission is detected after excitation by the narrow laser. In this case, at low temperatures, the up-hill energy transfer is inhibited, and hence, the light is emitted from the same absorbers, which are being selected by resonance with the excitation field. In the following, we do not consider the ΔFLN measurement, which is the difference of the fluorescence before and after the burn process.[54] This technique is beyond our theory.

When the excitation fluences in both HB and FLN are small, the measured field originates from the third order nonlinear response, i.e., the same response function as in the 2DES measurement. If the burn and measurement fields are "on" at the same time, the transient HB spectrum detects the third order susceptibility, which permutes the excitation and detection frequencies.[55] However, in 2DES, the excitation and detection frequencies are separated and independently controlled. The ingredients of 2DES, i.e., the ground state bleach, excited state emission, and excited state absorption interaction configurations, are the same as in HB,[55] while the excited state emission is the source of FLN; *vide infra*. Therefore, 2DES contains the same information as the transient HB. Since the electronic excitations as well as

spectral holes survive much longer than the time required to reach the electronically thermalized excited state, $t_2 = \infty$ delay time in 2DES is the proper parameter for comparison with HB and FLN.

For comparison with HB, we consider the vertical cross section (along ω_3) of the PP 2DES spectrum (Eq. (1)) with the burn frequency ω_B being the ω_1 frequency and the delay time $t_2 = \infty$. The FLN experiment matches with the vertical cross section of the ESE contribution of the PP 2DES spectrum with the excitation frequency matching ω_1 and $t_2 = \infty$,

$$FLN(\omega_3) = S_{ESE}(\omega_3, t_2 = \infty, \omega_B). \qquad (2)$$

Both $S_{\Sigma}(\omega_3, t_2 = \infty, \omega_B)$ and $FLN(\omega_3)$ depend on burn or excitation frequency correspondingly.

For completeness and the virtue of 2DES, we additionally introduce horizontal cross sections of the 2DES spectra. The cross section of ESE contribution corresponds to fluorescence excitation spectrum at a single ω_3 probe frequency and the cross section of PP 2DES corresponds to a scan of the burn energy over the absorption region while probing at a single frequency.

III. CONTRIBUTIONS TO 2DES SIGNALS FOR A THERMALIZED MOLECULAR SYSTEM

For simulation of the above-described spectra, the molecular complex under consideration is treated as an open quantum system. Quantum relaxation theory as well as theory of spectral line shapes is usually based on a model of linear coupling between the quantum system and its environment.[27,28,34,55] Such a system is described by a Hamiltonian of the displaced harmonic multidimensional oscillators. For most cases, the model is sufficient to describe complicated spectral line shapes. The theory may include Brownian overdamped ($10 < \omega < 100$ cm^{-1}) as well as damped vibrational modes ($\omega > 100$ cm^{-1}), even slow-to-static fluctuations can be included as low-frequency ($\omega < 10$ cm^{-1}) modes. The linear and non-linear response functions of a single chromophore have been exactly derived a while ago,[55] and this model has been extensively employed in spectroscopy modeling.

In the linear response, the homogeneous temperature-dependent spectral line shape comes from the function $g(t)$, which accounts for the thermal fluctuations of the nuclei. When the electronic transition is linearly coupled to the bath of harmonic oscillators, it is given by the correlation function of the energy gap fluctuations between the states of the system,

$$g(t) = \int_0^t d\tau_2 \int_0^{\tau_2} d\tau_1 C(\tau_1). \qquad (3)$$

The correlation function $C(t)$ completely describes the equilibrium properties of the harmonic oscillators. We denote Fourier transform of $C(t)$ by $C(\omega)$. Analytical calculation (see, for example, Section 7.8 of Ref. 28) shows that it is a real function which can be decomposed into even $C'(\omega)$ and odd $C''(\omega)$ parts, related by $C'(\omega) = C''(\omega) \coth(\beta\omega/2)$, where $\beta = T^{-1}$ is the inverse temperature and the Boltzmann constant is set to $k_B = 1$. The odd part $C''(\omega)$ is temperature independent and is used to define the fluctuation spectral density. As

the number of environment oscillators is essentially infinite, we can use $C''(\omega)$ as a continuous function. This function characterizes the amplitudes of energy fluctuations. The other spectral density $J(\omega)$, which directly comes from HB or FLN, is related to $C''(\omega)$ by

$$C''(\omega) = \omega^2 J(\omega). \qquad (4)$$

The absorption spectrum of a single pigment (chromophore) is given by a Fourier transform of the linear response function,

$$A(\omega) = \mu^2 \Re \int_0^\infty dt \, \exp(i\omega t - i\varepsilon_e t - g(t)). \qquad (5)$$

Here, ε_e is the vertical transition frequency and μ is the transition dipole. The asymptotic behavior of the $g(t)$ function as $t \to \infty$ governs the decay of the response function and the width of the absorption peaks. The spectral linewidth of all peaks (including the ZPL) becomes related to the long-time limit of $g(t) \to \gamma t - i\lambda t$ when t is larger than the decay time of the correlation function $C(t)$. Here, γ is the linewidth, and λ is the reorganization energy. Taking into account experimentally valid forms of spectral density $J(\omega)$, the electronic-only spectral peaks, i.e., the ZPL, get infinitesimally narrow (see also Sec. VI). However, this contradicts experiments, which show that the ZPL does have non-zero, temperature dependent linewidth. Despite this drawback, which affects essentially only ZPL, the linear-coupling model properly describes the phonon side bands and works well in spectroscopy simulations with ensemble averaging in wide range of temperatures. However, the shortcoming becomes crucial when one deals with site-selective techniques like HB or FLN at low temperatures.

It has been shown that the finite linewidth of the ZPL emerges from the simple quadratic coupling model.[56,57] As demonstrated in the Appendix, in the quadratic system-bath coupling model, the linear response function appears again in the usual form,[55] but the line shape function has two more terms

$$g(t) \approx \bar{\gamma}t + \bar{\sigma}^{(2)}\frac{t^2}{2} + g_l(t). \qquad (6)$$

Here, $\bar{\gamma}$ and $\bar{\sigma}^{(2)}$ are real-valued temperature-dependent constants while $g_l(t)$ is the line shape function of the linear coupling model. The values of the parameters $\bar{\gamma}$ and $\bar{\sigma}^{(2)}$ can be evaluated for the specific model of vibrational modes of the molecule. Thus, the quadratic coupling creates additional line broadening.[56,57] It can cause Lorentzian (when $\bar{\gamma} > \bar{\sigma}$) or Gaussian (when $\bar{\gamma} < \bar{\sigma}$) line shapes. We next assume that the ZPL line shape is Lorentzian.

In present work, we perform simulations at a constant temperature. We therefore use a constant value for the parameter $\bar{\gamma}$. We expect $\bar{\sigma}^{(2)} \ll \bar{\gamma}$ and ignore $\bar{\sigma}^{(2)}$ term. In our approach, the largest contribution to the overall line broadening will be caused by the linear coupling originating from $g_l(t)$; however, the Dirac-peaks in the spectra, e.g. ZPL, will now have finite linewidths. In the following, we therefore use the well-known expressions for the spectral line shapes coming from the linear-coupling model[4] but add the $\bar{\gamma}t$ term in the response functions to account for the ZPL linewidths.

When a number of pigments are under consideration, the bath may force electronic site energies of different pigments to fluctuate in a complicated pattern. However, since these fluctuations are relatively local in space, it is often assumed that the fluctuations of different pigments are uncorrelated. Thus, each chromophore is assigned a separate spectral density. Additionally, since the surrounding of different chromophores statistically is the same, the spectral densities of them are assumed to be the same as well. Due to resonant interpigment couplings, the delocalized exciton states experience diagonal as well as off-diagonal fluctuations.[4] The off-diagonal fluctuations are responsible for the excitation energy transport within the pigment-protein complex. The remaining diagonal fluctuations cause pure dephasing processes.

Since we study only two delay times, it is necessary to identify the relevant system states at these delay times. The delay $t_2 = 0$ describes the situation when populations did not start to evolve. Thus, the theory need not include transport during t_2, the dynamics is adiabatic, and the off-diagonal fluctuations in the exciton basis are included only via the exciton lifetime broadening during the delay times t_1 and t_3. The Redfield theory for off-diagonal fluctuations is sufficient to describe such case. During delay times t_1 and t_3 diagonal bath fluctuations are included by cumulant expansion approach.[4] For the delay time $t_2 = \infty$, all bath fluctuations have shorter correlation times than this time, and all possible correlations between the fluctuations at t_1 and t_3 delays have decayed. Additionally, the population in the electronic excited state (ESE and ESA pathways), created by the first two pulses, relaxes to the lowest exciton state, which at low temperature has infinite lifetime. The population dynamics is then completed and again the Redfield theory properly defines the final populations and the relevant broadenings related to the off-diagonal fluctuations.

This scenario corresponds to the doorway-window representation of the response function.[4,46,55,58] The expressions for the optical response functions relevant to 2DES are obtained by linearizing all terms in the phase function that contain t_2 time taking $t_2 \to \infty$. The response functions,[4] thus, factorizes into two terms: the doorway $\mathbf{D}(t_1)$ and the window $W(t_3)$ functions. Moreover, in the ESA and ESE contributions, the Green's function, giving the conditional probability of the exciton to hop from initial state e to final e' within the one exciton manifold during t_2, becomes $\mathbb{G}^{(N)}_{e'e',ee}(t_2 = \infty) = \delta_{e'e_1}$, where e_1 denotes the lowest exciton state. The final expressions of the response function producing the RP signal $S_I(\omega_3, \infty, \omega_1)$ are

$$R_I^{ESE}(t_3, \infty, t_1) = -i \sum_e \mathbf{D}_e^*(t_1) W_{e_1 g}^*(t_3), \tag{7}$$

$$R_I^{GSB}(t_3, \infty, t_1) = -i \sum_{e',e} \mathbf{D}_e^*(t_1) W_{g e'}(t_3), \tag{8}$$

$$R_I^{ESA}(t_3, \infty, t_1) = +i \sum_{e,f} \mathbf{D}_e^*(t_1) W_{e_1 f}(t_3). \tag{9}$$

For the NRP signal $S_{II}(\omega_3, \infty, \omega_1)$, the response functions are

$$R_{II}^{ESE}(t_3, \infty, t_1) = -i \sum_e \mathbf{D}_e(t_1) W_{e_1 g}^*(t_3), \tag{10}$$

$$R_{II}^{GSB}(t_3, \infty, t_1) = -i \sum_{e',e} \mathbf{D}_e(t_1) W_{g e'}(t_3), \tag{11}$$

$$R_{II}^{ESA}(t_3, \infty, t_1) = +i \sum_{e,f} \mathbf{D}_e(t_1) W_{e_1 f}(t_3). \tag{12}$$

The corresponding doorway and window functions are

$$\mathbf{D}_e(t_1) = \theta(t_1)\boldsymbol{\mu}_{ge}\boldsymbol{\mu}_{eg} \exp[-i\omega_{eg}t_1 - \gamma_{eg}t_1 - \bar{\gamma}t_1 - g_{ee}(t_1)], \tag{13}$$

$$\begin{aligned} W_{ab}(t_3) &= \theta(t_3)\boldsymbol{\mu}_{ab}\boldsymbol{\mu}_{ba} \exp[-i\omega_{ba}t_3 - \gamma_{ba}t_3 - \bar{\gamma}t_3 \\ &\quad - g_{aa}(t_3) - g_{bb}(t_3) + g_{ba}(t_3) + g_{ab}(t_3) \\ &\quad + 2i(\lambda_{ba} - \lambda_{aa})t_3]. \end{aligned} \tag{14}$$

Here, $\theta(t)$ is the Heaviside function, $\omega_{ab} = \varepsilon_a - \varepsilon_b$ is the transition frequency, $\gamma_{ab} = \frac{1}{2}(\tau_a^{-1} + \tau_b^{-1})$, where τ_a is the lifetime of a state a, $g_{ab}(t)$ is the line shape function given by the correlation function of the energy fluctuations of the states a and b, $\lambda_{\nu\nu'}$ is the reorganization energy, and $\bar{\gamma}$ is the damping constant originating from the quadratic system-bath coupling (see Eq. (6)). Of course, in simulations, one needs to include the orientational averaging of the transition dipoles over the arbitrary orientations of the whole system.

At delay time $t_2 = 0$, we should observe equivalents of coherent PP measurements and the bath properties with respect to the electronic ground state. We have incorporated the damping constant of quadratic coupling $\bar{\gamma}$ into the third order response functions used to obtain 2DES with $t_2 = 0$ delay as well. These response functions are used as described in Ref. 4.

IV. SPECTRA OF A SINGLE CHROMOPHORE

Before studying the molecular dimer, let us inspect the 2DES of a single chromophore at low temperature. It consists of adiabatic ground and excited electronic states. A damping constant $\bar{\gamma}$ is set to $\bar{\gamma} = 1.5$ cm^{-1} for all coherence delay times. The profile of the spectral density corresponds to the particular spectral content of the fluctuating environment. Additionally, its functional form defines the convergence and correct asymptotic behavior. The log-normal function has been suggested as most relevant to describe the spectral density for photosynthetic pigment systems.[44] For further simulations, we chose the spectral density extracted from experiments on recombinant CaWSCP, which had been fitted with three log-normal functions (Figure 1).[36,44] Here, we use the spectral density of the lowest energy dimers (that due to disorder cannot transfer energy) in CaWSCP.[36] In Figure 1, the spectral density is presented in two forms, $J(\omega)$ and $C''(\omega)$. Another environment related characteristic is the distribution of the static energy disorder which we represent as a Gaussian function with variance $\sigma = 50$ cm^{-1}. The temperature used in the simulations throughout the paper is T = 0.1 K. (It is taken above zero for proper numerical convergence.)

We start with simulations of the simplest spectroscopic experiment—the linear absorption (LA) spectrum calculated Eq. (5). The results of these simulations are presented in
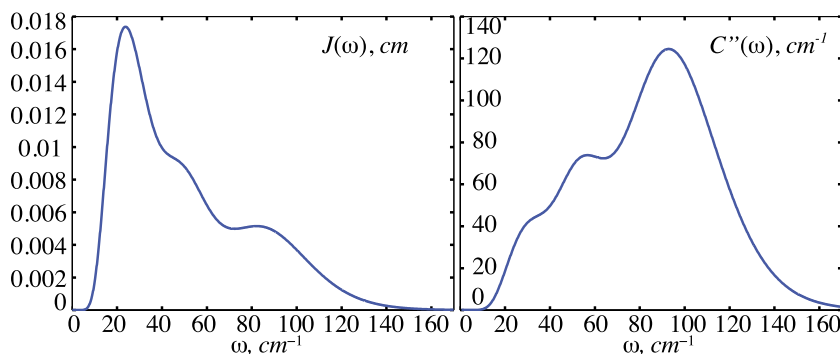
FIG. 1. Left: Fluctuation spectral density $J(\omega)$ extracted from ΔFLN of WSCP with Chl a and fitted with three term log-normal function.[44] Right: The same spectral density in the form $C''(\omega)$.

Figure 2 for two cases: without static energy disorder (left plot) and with the static energy disorder (right plot). Simulated LA without static energy disorder demonstrates clearly the sharp ZPL and the PSB. The side band of the absorption spectrum clearly reflects the $J(\omega)$ spectral density, because of the small HR overall parameter, $s_h = 0.81$, and reorganization energy $\lambda = 41.2$ cm^{-1}. However, the model without static disorder does not match with any real experimental situation. Adding the inhomogeneous broadening naturally hides the fine structure.

We proceed to the 2DES simulation of the chromophore. To visualize the fine structure of the spectrum we again start with models without static disorder. The RP and NRP spectra and their sum (PP) are shown in Figure 3. All plots are made with 20 contours. Note, for a two-level system, only GSB and ESE contributions are possible.

Similar to absorption, we can distinguish the ZPL feature (as it is a Lorentzian-like 2D peak, we will denote it as a zero-phonon-peak - ZPP) and the phonon-related features, which make quite complicated extended peak shape. At such low temperature, the sharp ZPP dominates the spectra. Notably, the ZPP is much stronger compared with the phonon side-peaks. Therefore, in order to see more features in 2D spectra of Figure 3, only 3% of the intensity is plotted.

The RP and NRP spectra at zero delay time show very different features related to bath spectral density: most notably, the NRP spectrum is symmetric along the diagonal, and phonon peaks are mostly localized outside the diagonal. The RP features of the spectral density are widely distributed both on the diagonal and off-diagonal regions. This can be rationalized by keeping in mind the photon echo phenomenon, i.e., that static fluctuations completely rephase thus leading to features exactly on the diagonal line in the RP spectrum. While there are no static fluctuations in the present case, the lowest frequency components in the spectral density partially

rephase to a large extent giving strong features close to the diagonal. The high-frequency oscillators do not rephase and their features largely deviate from the diagonal line. This leads to overall horizontally extended (yellow in the figure) phonon-related feature. Since the RP spectrum is overall more widespread than NRP spectrum, its amplitude becomes smaller than the NRP amplitude. We also show the maximum intensity value of each 2D plot relative to the maximum intensity of PP at $t_2 = \infty$. As we always model the same system, these intensity values can be compared. It turns out the PP spectrum at $t_2 = 0$ is dominated by the NRP component.

At the infinity delay time, the bath relaxes to the potential minimum of the electronic excited state, and as a result, the phase information becomes lost, and RP and NRP contributions become equal in amplitude. The rephasing phenomenon disappears. The RP and NRP spectra are flipped vertically. Hence, the resultant PP appears very symmetric. At this delay time, the traces of the spectral density become clearly identifiable: the features above ZPP (along the diagonal) appear from the GSB and below the ZPP from the ESE contributions, which is the mirror image of the GSB.

We next include the static energy disorder (Figure 4; the layout corresponds to the one of the Figure 3). The plots are presented with 100% amplitude. The maximum intensity value relative to the maximum intensity of PP at $t_2 = \infty$ is shown on each plot.

RP spectra are dominated by the sharp diagonally elongated quasi-1D Gaussian ZPP at both delay times. It is created by the narrow disorderless ZPP with excitation energy distributed along the diagonal. As the rephasing phenomenon is perfect for static fluctuations, the peak is inhomogeneously elongated only along the diagonal. The bath-related phonon features are also distributed along the diagonal; however, they become stronger below the diagonal. Again, this is related to weakening of the rephasing phenomenon as the phonon
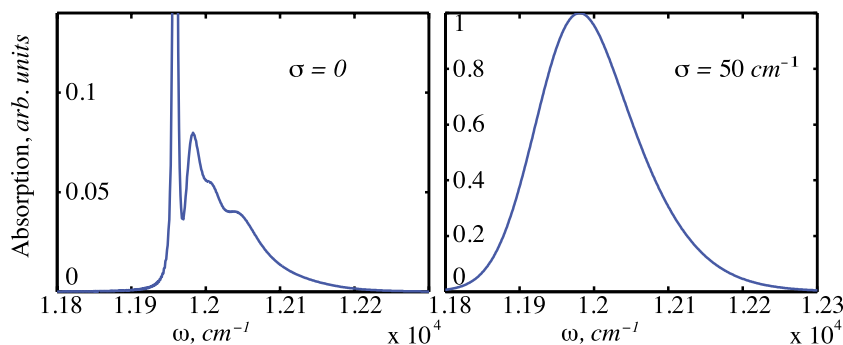

FIG. 2. Absorption spectra of a chromophore coupled to a fluctuating environment with spectral density as presented in Figure 1. Left: no static energy disorder (maximum amplitude is cut at 14%); right: with a static energy disorder from Gaussian distribution with variance $\sigma = 50$ cm^{-1}.
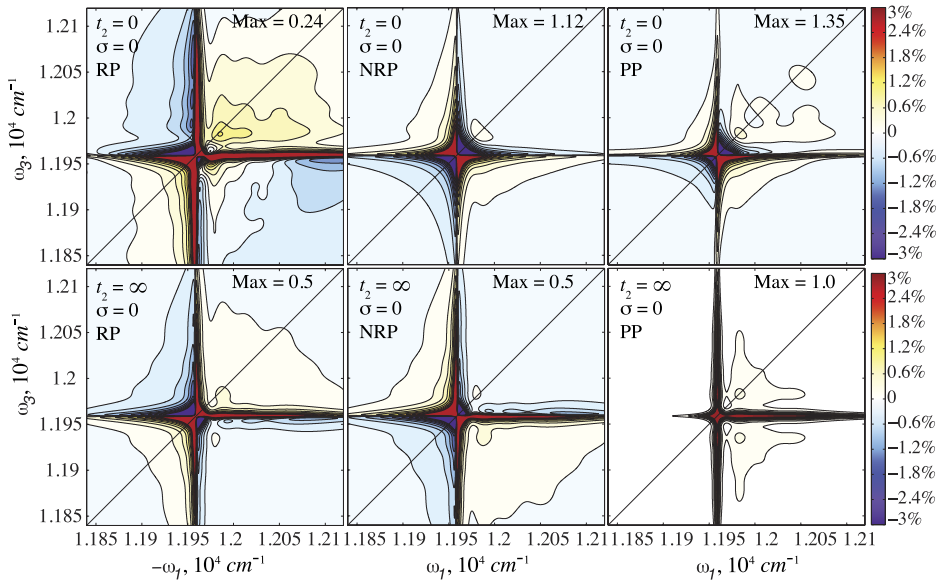
FIG. 3. 2D real part (absorptive signal) of RP, NRP, and PP spectra of a single two-level chromophore coupled to a fluctuating environment. No static energy disorder included. Top row: $t_2 = 0$; bottom row: $t_2 = \infty$. Each spectrum shows 3% of a maximum intensity. Maximum value relative to the maximum of PP signal at $t_2 = \infty$ is shown in the top right corner of each frame. T = 0.1 K.

frequencies become higher. The NRP signal, however, does not show any fine features which would reflect the spectral density. In the NRP plots, the static disorder widens the peak in all directions and produces essentially featureless 2D Gaussian peak, which merely shifts down due to complete bath relaxation at $t_2 = \infty$ showing the Stokes shift. As the amplitudes of the RP spectra are now much higher than those of the NRP signals, the resultant PP spectra are now dominated by the RP contributions. Note, that the maximum value of the signal denoted in the upper right of each spectrum differs nearly two times between $t_2 = 0$ and $t_2 = \infty$ for the RP and PP spectra. This is due to wider distribution of the intensity at zero delay. We thus find that the RP part clearly dominates the PP spectrum at low temperatures.

At $t_2 = \infty$ delay, the 2D PP spectrum consists of the relaxed GSB and relaxed ESE contributions which are shown separately in Figure 5. The GSB is completely symmetric along the diagonal with bath features appearing above and below the diagonal. However, the phonon feature in ESE is completely below the diagonal. This demonstrates that GSB and ESE can be completely reconstructed from PP by taking the difference of the spectrum above and below the diagonals.

2D spectra however contain much more information than visually seen in 2D plots. Some of it can be extracted from different cross sections. Vertical and horizontal cross sections, as marked on the PP plots (Figure 4) and the ESE plot (Figure 5), are presented in Figure 6. The ESE cross sections strongly resemble the absorption without disorder (Figure 2) where the bath spectral density (Figure 1) is clearly seen. However, since ESE vertical cross section corresponds to fluorescence experiment, this feature is at the lower energy side. The PP cross sections at $t_2 = \infty$ look similar to ESE though it possesses GSB features as well. Note, that ESE cross sections have sharp main peak and a band on one side of the peak only. Thus, in the PP cross sections, weaker contributions on the other side of the main peak originate from the GSB signal which is highly symmetric in the 2D plot. This cross section shows bath features in the ground state (GSB above
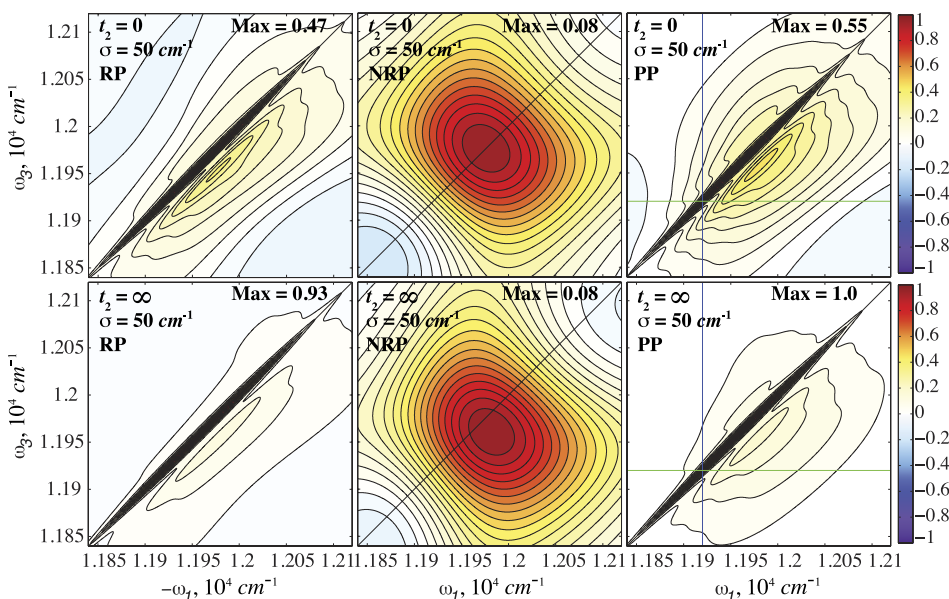

FIG. 4. 2D real part (absorptive signal) of RP, NRP, and PP spectra of a single two-level chromophore coupled to a fluctuating environment with a static energy disorder from Gaussian distribution with variance $\sigma = 50$ cm^{-1}. Top row: $t_2 = 0$; bottom row: $t_2 = \infty$. All plots are with 100% intensity. On PP plots, the vertical (blue) and horizontal (green) cross sections are marked. These are presented in Figure 6. Maximum value relative to the maximum of PP at $t_2 = \infty$ is shown in the top right corner of each frame. T = 0.1 K.
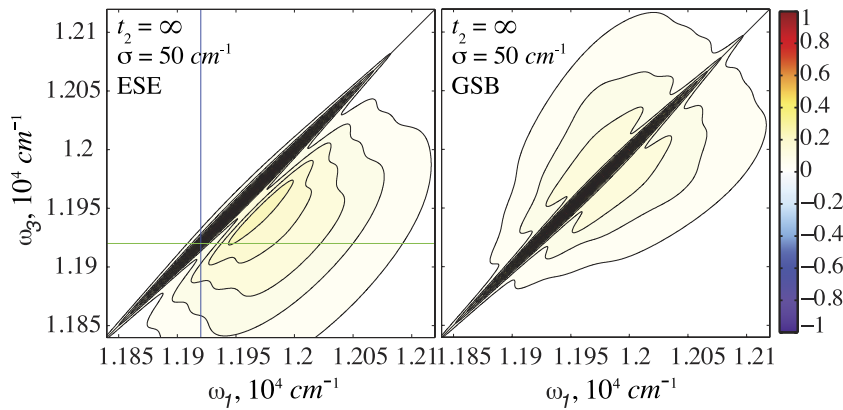
FIG. 5. 2D real part (absorptive signal) of PP components ESE and GSB of a two-level system coupled to a fluctuating environment with a static energy disorder from Gaussian distribution with variance $\sigma = 50$ cm^{-1} at $t_2 = \infty$. On ESE plot, the vertical (blue) and horizontal (green) cross sections are marked. These are presented in Figure 6. Maximum values of ESE and GSB components before renormalization are similar. T = 0.1 K.

ZPP) and in the excited state (PP below ZPP minus GSB, or ESE only).

In the cross section of the PP spectrum at zero delay, the bath-related features are much stronger with respect to the ZPP than in the $t_2 = \infty$ case. This is especially visible in the horizontal cross section, which closely matches with the absorption line shape without disorder. Note that at zero delay time, the bath is still in equilibrium with the ground state of the system. Thus, the ESE spectrum contains phonon features not only below but also above diagonal (not shown), because the bath does not relax to the equilibrium on the electronic excited state. Therefore, in the PP cross section at zero delay, the bath-related features contain contributions from both ESE and GSB components on either side of the ZPP. These features observed in the cross sections at $t_2 = \infty$ reflect the experimental data and traditional simulations of the single chromophores for both FLN and HB techniques (see, for example, Refs. 31, 35, 54, 59, and 60). Of course, the experiments on solutions of chromophores usually do not have the structured phonon spectral densities as the one obtained from the CaWSCP we use here.

V. SPECTRA OF A MODEL DIMER

A. Description of a dimer model

To analyze excitonic effects, we next study a molecular homodimer. We have tuned its parameters in such a way

that the simulated spectra of our model qualitatively reflect the spectral properties of CaWSCP protein. The main reason why we have chosen WSCP as a reference for the dimer model is due to the clearly structured profile of its spectral density. This profile we seek to trace in the spectral line shapes, whereas the values of other parameters of the homodimer model are tuned in order to have clearer overall picture. The CaWSCP protein was proclaimed one of the simplest pigment-protein complexes as it contains a dimer of strongly interacting chlorophyll chromophores,[61] though it was suggested recently[42] that both LvWSCP and CaWSCP most likely contain two similar dimers of Chl a.

We next study a homodimer of excitonically coupled two-level chromophores with site energies of 14 800 cm^{-1} and coupling strength $J = 85$ cm^{-1}. This gives the excitonic splitting of the energy levels in the system of 170 cm^{-1} (when taken without static disorder). The angle between transition dipoles in our model dimer is taken 47°. This value is different from the angle within the strongly coupled dimers present in a tetrameric WSCP obtained from the crystal structure, which is found to be approximately 28°; however, the angle of 47° in our simple dimer model leads to a ratio of peak amplitudes in absorption spectrum close to that of the WSCP protein. Thus, only qualitative comparison between our model and WSCP can be made at this time.

The excitonic system is described by Frenkel exciton model. It contains one ground state, two single exciton states, and one double exciton state. Additional to the single
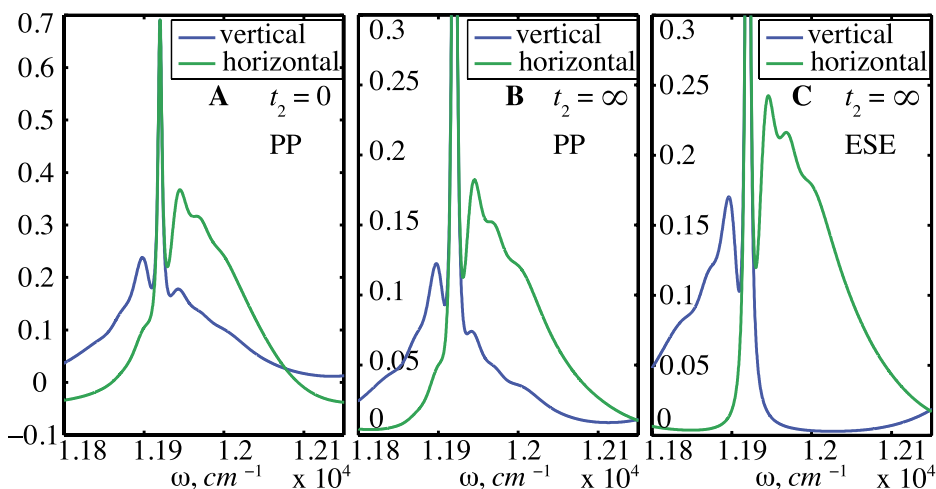

FIG. 6. Vertical and horizontal cross sections in the lower energy region as marked in the Figures 5 and 4. A: cross section of PP spectrum at $t_2 = 0$; B: cross section of PP spectrum at $t_2 = \infty$; C: cross section of ESE contribution at $t_2 = \infty$. Blue—vertical and green—horizontal cross sections. Slight amplitude increases at the edges of the spectra are due to numerical FFT aliasing.

chromophore system, the dimer experiences ESA due to the double exciton state corresponding to electronic excitation of the two chromophores. In the simplest approach, it is usually assumed that the energy of the double exciton state is equal to the sum of energies of the chromophore excitations. However, this approach does not take into account that different electronic configurations of one of the chromophores (electronic excited vs electronic ground) affect the excitation energy of the neighboring chromophore. Therefore, the double exciton energy may have an additional shift, denoted as the bi-exciton binding energy (sometimes also denoted as the quartic coupling).[62] By putting side by side our simulated 2DES spectra along ω_3 axis (described below) and HB experiments of the recombinant CaWSCP,[36,37] we found that the qualitative similarity of spectra is obtained when the binding energy is roughly +100 cm^{-1} (double exciton energy band is shifted up by this value). See Sec. VI for more details.

Following simulations of Sec. IV, we add Gaussian static energy disorder to chromophore site energies with variance $\sigma = 50$ cm^{-1}. However, the dimer model allows additional degree of freedom describing how the energies of the chromophores are distributed with respect to each other. Three types of the static disorder can in principle be possible and will be considered. (i) Correlated static energy disorder corresponds to situation when the site energies of chromophores in the system experience the same static fluctuations. This case can be modeled by applying the convolution of spectra with Gaussian spectral profiles for all interaction configurations. The convolution in time domain is equivalent to multiplication by a factor $\exp(-\sigma^2(t_1 \pm t_3)^2/2)$, where "+" sign is for NRP and "−" is for RP contributions. In the (ii) case of uncorrelated static energy disorder, the site energies fluctuate independently from each other, while in the (iii) case of the anti-correlated disorder, the site energy shifts for two chromophores are of the same value but have opposite signs. Both (ii) and (iii) cases are modeled explicitly by adding random energy shifts to pigments from a Gaussian distribution and making numerical ensemble averaging. The ensemble of the uncorrelated and anti-correlated static energy disorder is composed of at least 10 000 members to obtain smooth spectral shapes.

It must be taken into consideration that the Förster, Redfield, and modified Redfield theories[27,28,63] are approximate for photosynthetic pigment-protein complexes, because couplings between the pigments are on the same order as the amplitudes of the environment fluctuations. In this case, energy level crossing (degeneracy) of electronic states is unavoidable, and only the non-perturbative theories like hierarchical equations of motion[29,64] provide exactly correct dynamics. However, the excitonic splitting in our model is larger than most of the frequencies in the bath spectral density with the current set of parameters. Therefore, the Redfield approach used in this paper is a proper approximation.

B. Absorption in three cases: Correlated, uncorrelated and anti-correlated disorder

Absorption spectrum of this system at low temperature is presented in the Figure 7. The spectra for the cases of correlated and uncorrelated disorders are dominated by inhomogeneous broadening. Orientations of transition dipoles lead to H-type aggregate features with the higher exciton state more intensive than the lower one. The intensity of the lower exciton state is only about 20% of that of the upper state. In the LA, no structure of the spectral lines (ZPL and PSB) is seen in the correlated and uncorrelated case of the disorder. Correlated disorder results in wider peaks in LA spectrum, whereas peaks are slightly narrower and thus better separated for uncorrelated static energy disorder model. (The gap between two exciton transitions is well distinguished.)

The case of anti-correlated disorder makes very special line shapes at these low temperatures. We find extremely narrow well separated excitonic peaks. This can be rationalized taking into account that (i) the homogeneous linewidth is very narrow, (ii) the mean excitation energy for the dimer is always constant because the energies of the two pigments shift up or down by the same amount in different directions, and (iii) the coupling J between the pigments introduces the energy gap between excitonic states which cannot be smaller than $2|J|$. In present model, it means that the excitonic splitting is at least 170 cm^{-1}, whereas the spectral density used (see Figure 1) at this frequency is approaching zero. The exciton energy distribution, thus, is peaking at the splitting $2|J|$ and it has zero density of states inside the gap. This discontinuity is filled in the absorption spectrum only by homogeneous line shapes, which are only few cm^{-1} wide. Therefore, the present case reveals the homogeneous line shapes (ZPL and PSB)
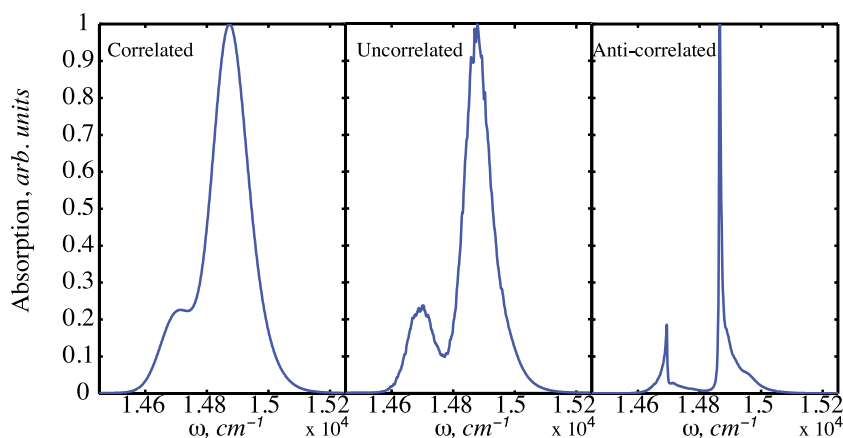

FIG. 7. Absorption spectra of the dimer model system with a static energy disorder from Gaussian distribution with variance $\sigma = 50$ cm^{-1}. Left: correlated static energy disorder; middle: uncorrelated static energy disorder; right: anti-correlated static energy disorder model. T = 0.1 K.

inside the excitonic gap. Outside the gap, the disorder makes smooth decay of absorption intensity going away from the excitonic gaps. Whether the anti-correlated model is realistic given this result is a separate question of course and it is addressed in Sec. VI.

C. Modeling of 2DES spectra for the dimer

Next, we describe the 2DES spectra of the molecular homodimer. Keeping in mind the features seen for the single chromophore case, we start immediately with the PP spectra including static energy disorder of the three types.

The 2D PP spectra with three static energy disorder models at two different delay times $t_2 = 0$ and $t_2 = \infty$ are presented in Figure 8. The ratio of the intensities of the absorption peaks is further enhanced in the diagonal peaks of the 2DES. For example, in the 2D PP at $t_2 = 0$, the lower exciton band is so weak that it is invisible if the 2D plot is presented with 100% intensity and 10 contours. Therefore, the plots cut at 20% of the maximum intensity and then renormalized to 1 are presented in the Figure 8 for

the correlated and uncorrelated static energy disorder cases shown in the top and middle rows correspondingly. In the case of anti-correlated disorder, the peaks are so sharp that the 2D plots in Figure 8 (bottom row) are cut at 5% of the intensity in order to show underlying line shape features.

In 2D correlation plots (2DES at $t_2 = 0$), two diagonal peaks and two cross-peaks originate from the ESE and GSB contributions (positive). The negative ESA signal is seen between the upper diagonal peak and lower cross-peak gaining dipole strength from the upper exciton band but shifted up from the lower cross-peak due to the 100 cm^{-1} bi-exciton binding. The weaker ESA signal (positive feature) above upper cross-peak is up-shifted as well.

These features are observed in all PP plots simulated with all three types of the static energy disorder at $t_2 = 0$. The correlated and uncorrelated disorder cases look rather similar. First of all in all cases, the ZPP features are sharp and clear in the diagonal peaks. Their elongation along the diagonal clearly reflects the disorder-induced distribution. Again as it was in the case of the single chromophore, here the 2D PP spectra are dominated by the RP contributions.
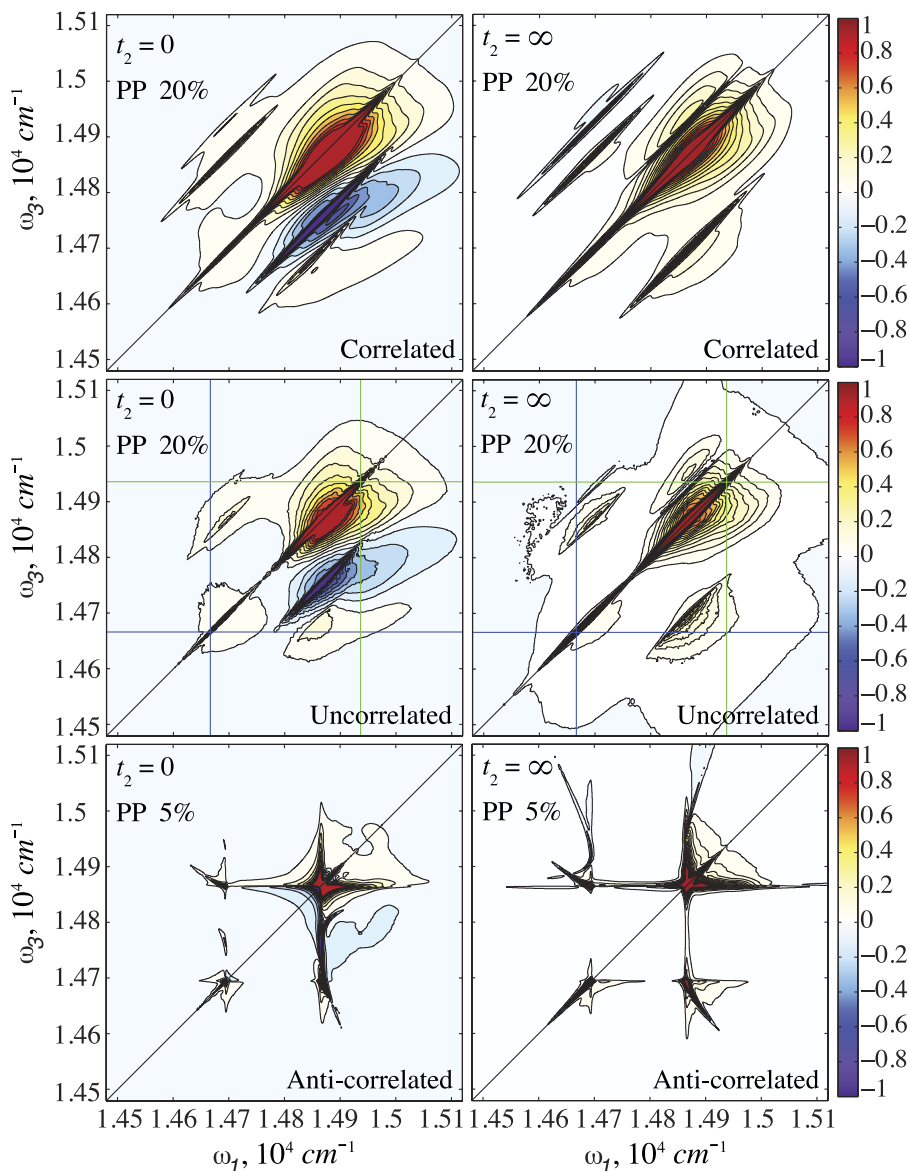

FIG. 8. 2D real part (absorptive signal) of PP of the model dimer calculated with three types of the static energy disorder: top row—correlated static energy disorder, middle row—uncorrelated static energy disorder, bottom row—anti-correlated static energy disorder model. Left: $t_2 = 0$; right: $t_2 = \infty$. The maximum intensity is cut at the value shown on each plot in per cents. Plots are then normalized to 1. All plots contain 20 contours. T = 0.1 K. On the plots simulated with uncorrelated static energy disorder the cross sections are marked. These data are presented in the Figure 10.

The diagonal peaks cannot distinguish between the correlated and uncorrelated disorder cases. However, the cross-peaks demonstrate distinct properties. The cross-peaks of the correlated disorder case contain sharp diagonally elongated ZPP-like profiles that follow the diagonal peaks. However, in the case of the uncorrelated disorder, the cross-peaks are broadened asymmetrically by the disorder anti-diagonally as well.

The plot obtained using the anti-correlated disorder model looks most distinct. The relative positions of peaks in the 2D spectrum are the same but the ZPP shapes and cross-peaks are strikingly different than in other disorder cases. As in the LA spectrum, the ZPP is still very sharp clearly distinguishable in the PP spectrum. There are elongations of the diagonal peaks along diagonal outwards from the center of the spectrum produced by anti-correlated site energy shifts. However, the inhomogeneous broadening of the diagonal peaks still is much smaller than in the other disorder cases. The cross-peaks, however, are elongated not in parallel with the main diagonal (like in correlated disorder case) but in more or less anti-diagonal direction outwards from the center, thus, explicitly indicating the anti-correlated fluctuations. The shape of the negative feature of the ESA signal below the upper diagonal peak is poorly resolved.

Let us turn to the $t_2 = \infty$ 2D plots. In this case, the system population before interaction with the third pulse is either in the ground state (in GSB) or in the lowest excited state (in ESE and ESA). This redistributes the transition dipole strength in the system. Now, neither upper diagonal peak nor upper cross-peak has ESE contribution. The ESA contribution

(negative feature) is seen only above the upper diagonal peak and upper cross-peak. Plots obtained with correlated and uncorrelated static energy disorder appear quite similar at first sight. More careful examination, however, shows that the ZPP trace on the diagonal is sharper in the uncorrelated disorder case while the cross-peaks, on the contrary, are sharper in the correlated disorder case. The broadening of the cross-peaks in the uncorrelated case is asymmetric, with smooth decay outside from the diagonal, while sharper inside. In the case of the anti-correlated disorder, the cross-peak elongations across the diagonal become clearly visible. Moreover, the ESA peak shapes become more resolved above the upper cross-peak.

These features are very clearly pictured in Figure 9 where the contributions GSB, ESE, and ESA of PP signal for $t_2 = \infty$ obtained with three types of the static energy disorder are shown. All spectra are presented with 20 contour plots. The separate representation allows one to see explicitly the intensity distribution of various contributions.

At this delay ($t_2 = \infty$), ESE and ESA signals always originate from the same relaxed lowest exciton state. The ESE contribution is then positioned below the lowest one-exciton energy, and the ESA signal is above the highest one-exciton state. However, the GSB signal does not select any excited state, and the peak distribution is approximately symmetric with respect to the diagonal.

The profiles of ZPP on various peaks reflect different static energy disorder models. As already noticed above, the general appearance of the GSB and ESE contributions obtained with correlated disorder model resembles the single molecule spectra. In the correlated static energy disorder case,
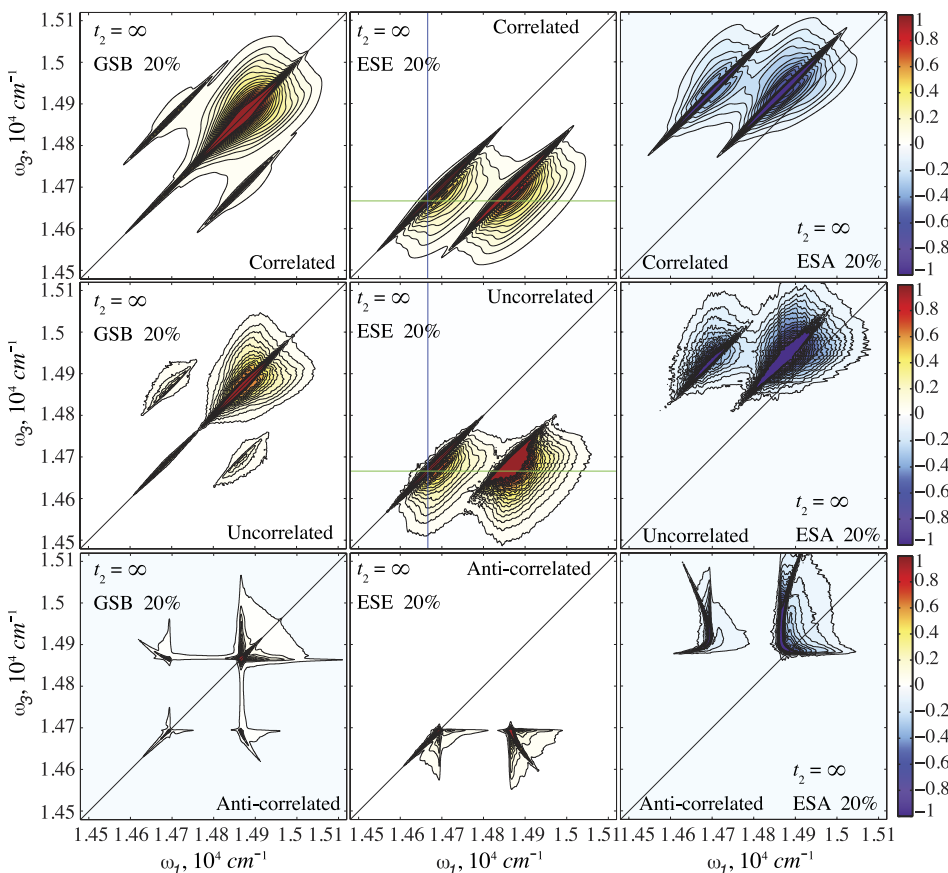

FIG. 9. GSB, ESE, and ESA contributions (the real part (absorptive signal)) to PP signals simulated at $t_2 = \infty$ presented in the Figure 8. All spectra modeled with three types of the static energy disorder: top row—correlated static energy disorder, middle row—uncorrelated static energy disorder, bottom row—anti-correlated static energy disorder model. All plots contain 20 contours. T = 0.1 K. On the ESE plots simulated with correlated and uncorrelated static energy disorder the cross sections are marked. These data are presented in the Figure 11.

the energy gap between excitonic states remains constant, produced solely by constant coupling. The fluctuating site energies lead to fluctuating average one-exciton band energy. Hence, the diagonal peaks are fluctuating in the same way as in the case of isolated pigments. The picture is opposite in the case of anti-correlated fluctuations. In this case, the average one-exciton band energy remains constant but the disorder produces variable splitting of the excitonic energy gap, which can be only larger or equal than the excitonic splitting of the correlated disorder case. The two-exciton energy remains constant in the anti-correlated disorder case. This leads to specific elongation of GSB and ESE cross-peaks outwards from the average one-exciton energy (approximately in the center of the plots) and to very specific shapes of the ESA contributions with anti-correlated static energy disorder model.

Unsurprisingly, the uncorrelated disorder model, being in between the cases of fully correlated and fully anti-correlated cases, leads to peak shapes being similar to the correlated-type patterns, however, having some features of the anti-correlated-type patterns. In particular, the cross-peaks still have sharp elongations along the diagonal, however, elongation across the diagonal away from the diagonal emerges.

As the ZPP features are clearly visible on the diagonal peaks, the remaining background in the diagonal peaks necessarily comes from the bath spectral density. Thus, similar to the single chromophore case, the PSB profiles surrounding the ZPP on the diagonal peaks are reminiscent of the $J(\omega)$ spectral density functions. We investigate this in more details by checking various cross sections of these 2DES plots.

D. Cross sections of the 2DES spectra for the dimer

The vertical and horizontal cross sections of the 2D PP plot at $t_2 = 0$ and $t_2 = \infty$ in the case of uncorrelated static energy disorder are shown in Figure 10. The cross sections are made at the lower energy side of the lowest energy band (i.e., the lowest exciton state) and higher energy side of the higher energy band and are marked on the corresponding 2D PP plots in Figure 8 middle row. The frequencies of the cross sections are chosen to approximately correspond to the ones, which are used in Ref. 37. Please note, that the cross sections are plotted using inverse amplitude sign in comparison to the PP spectra in order to present the spectral holes as negative features in accord with the HB measurements.

In the cross sections made at lower frequency (14 666 cm^{-1}, blue line in the plots), the lower energy signal comes from the lower diagonal peak and higher energy signal from the cross-peaks: the upper cross-peak in the vertical cross section and the lower cross peak in the horizontal cross section. Whereas in the cross sections made at higher frequency (14 936 cm^{-1}, green line in the plots), the lower energy signal comes from the cross-peaks: the lower cross-peak in the vertical cross section and the upper cross peak in the horizontal cross section; and higher energy signal originates from the upper diagonal peak.

The vertical cross sections of the PP spectrum at $t_2 = \infty$ are related to absorption bleaches. Since our theory does not consider close-lying anti-holes typically observed in the NPHB spectra, the bleaches shown in Figure 10(c) represent transient excitonic features. Thus, the vertical cross section spectra extracted from the 2DES maps, though similar to the experimental HB spectra in Ref. 37 (i.e., they include all expected features), cannot be straightforwardly compared to the experiment, since the experimental spectra were obtained for a tetramer, and most likely are contributed to by both non-photochemical and photochemical holes (unpublished data). Besides, HB spectra shown in Ref. 37 contain contribution from the sharp vibronic holes not taken into account in our modeling studies. However, the bleach (or spectral ZPL holes as well as surrounding PSBs) formed by absent equilibrium absorbers is of the same origin in simulations and experiment.

Then, the vertical 2DES sections can be in principle interpreted using low-temperature terminology as follows. When "burn" frequency is $\omega_1 = 14\,666$ cm^{-1}, one may distinguish the following HB-type features in the cross section going from the low to high energies: pseudo-PSB, spectral hole with weak real PSB, and then broad negative feature peaking at $\omega = 14\,838$ cm^{-1} originating from the cross-peak, which can be interpreted as the "satellite holes" of excitonic origin, followed by positive "anti-hole" at $\omega = 14\,897$ cm^{-1} created by ESA contribution. When excitation frequency $\omega_1 = 14\,936$ cm^{-1},
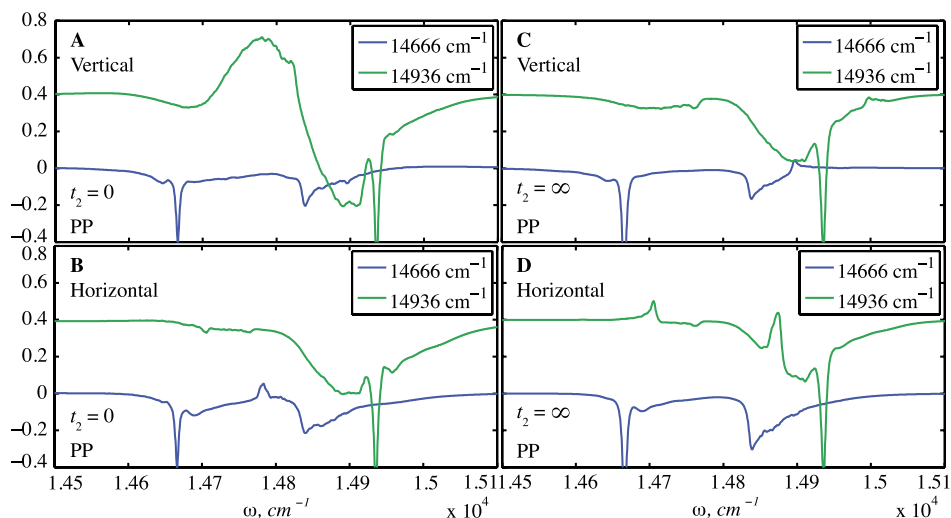

FIG. 10. Vertical and horizontal cross sections of the real part (absorptive signal) of PP spectra of the model dimer calculated with uncorrelated static energy disorder. Left: $t_2 = 0$; right: $t_2 = \infty$. Top row: vertical cross sections; bottom row: horizontal cross sections. C plot cross sections correspond to HB spectra. Cross-sections are presented with the opposite sign of the amplitude. Blue—cross section made at lower frequency and green—cross section made at higher frequency. Cross section frequency values in cm^{-1} are shown in the plots.

the cross section contains following features: shallow "satellite holes" around $\omega = 14\,700$ cm^{-1} with distinguishable feature at $\omega = 14\,755$ cm^{-1} originating from lower cross-peak and thus created by excitonic relaxation of the upper exciton band, then broad deeper "satellite hole" about $\omega = 14\,896$ cm^{-1}, originated from the phonon features of the upper exciton band, with narrow main hole on its high energy side followed by a weak "anti-hole" at $\omega = 14\,994$ cm^{-1} created by ESA of the upper exciton band.

Again, as in the one molecule case, we can extract fluorescence features from the third order response simulations. The ESE pathway separately at $t_2 = \infty$ corresponds to the relaxed fluorescence spectrum, which is equivalent to FLN at low temperatures. The 2D ESE spectra simulated for $t_2 = \infty$ are in Figure 9. The cross sections at $\omega_1 = 14\,666$ cm^{-1} of the ESE contribution are shown in Figure 11 for the cases of correlated and uncorrelated disorders. As seen in the 2D ESE plots for $t_2 = \infty$, only the lower diagonal peak and the corresponding cross-peak are relevant. Thus, the vertical cross section (Figure 11, blue) contains only one feature originating from the diagonal peak. Whereas the horizontal cross section shows two features—first (at $\omega = 14\,666$ cm^{-1}) from the diagonal peak and second (at $\omega = 14\,838$ cm^{-1}) from the cross-peak.

The vertical cross sections, corresponding to FLN experiment, look very similar in both correlated and uncorrelated disorder cases, and even in the case of a single molecule (Figure 6). In the horizontal cross sections, the first feature is again similar in both disorder cases and in the single molecule case, but the second feature appears different. Of course, the latter feature is not present in the one molecule case. So in both vertical and horizontal cross sections of the diagonal peak, the ESE imprints the fluctuation spectral density $J(\omega)$. The correlated and uncorrelated static energy disorders are best distinguished in the cross-peak features.

VI. DISCUSSION

A. Limitations of the linear system-bath coupling model

Nuclear dynamics play an essential role in electronic excitation dynamics in molecular systems. In particular, the photosynthetic pigment-protein complexes are constructed out of few types of pigments; however, the functionality of the complexes, shaped by the surrounding protein static configurations and dynamic fluctuations, is very diverse, ranging from light harvesting and photoprotection to charge separation.[65] Three types of nuclear dynamics are usually distinguished. First of all, these are the localized intramolecular vibrations

of the pigments themselves. Often, these are well distinguishable resonances above 200 cm^{-1} determined by Raman spectroscopy studies, ΔFLN and HB experiments.[31,66] At such frequencies, they are at rest in thermal equilibrium, and their dynamics is initiated by electronic transitions. Second type of nuclear dynamics is caused by fluctuating surrounding molecules or protein groups often referred as phonons.[31] Their frequencies are below room-temperature thermal energy so they perform Brownian fluctuations. However, their frequency distribution is not uniform, so the created noise is colored. The so-called phonon spectral density function characterizes the distribution. Various theoretical models are often assumed for the spectral density fluctuation profile. The Ohmic spectral density is the "physically sound" model which assumes the linear relation $C''(\omega) \propto \omega$ at low frequencies which is exponentially terminated at high frequencies.[11] The linear growth at low frequencies is in line with the white noise model since the real part of the correlation function is then proportional to $C'(\omega) \propto T$ and is independent of frequency. The other similar spectral density is of the overdamped Brownian oscillator bath model,[4,55] which is constructed by requesting the exponentially decaying time correlation function (more specifically, its real part). This leads again to the same $C''(\omega) \sim \omega$ dependence at low frequencies. However, specific low temperature HB and FLN experiments have demonstrated that low-frequency behavior of the spectral density should be different.[44] Additionally, in these models, we obtain a diverging function $J(\omega) \sim \omega^{-1}$, which leads to diverging total HR factor s_h (see below). Hence, the simple physical models do not necessarily demonstrate correct behavior of the nature.

The total reorganization energy,

$$\lambda = \int_0^\infty \frac{d\omega}{\pi} \frac{C''(\omega)}{\omega} = \int_0^\infty \frac{d\omega}{\pi} \omega J(\omega), \qquad (15)$$

and the total HR parameter, which is a dimensionless quantity,

$$s_h = \int_0^\infty \frac{d\omega}{\pi} \frac{C''(\omega)}{\omega^2} = \int_0^\infty \frac{d\omega}{\pi} J(\omega), \qquad (16)$$

are well-determined experimental quantities. They both provide finite numbers, so both integrals converge. Assuming an analytical relation at small frequencies,

$$C''(\omega) = a_n \omega^n \mid_{\omega \to 0} \qquad (17)$$

or

$$J(\omega) = a_n \omega^{n-2} \mid_{\omega \to 0}, \qquad (18)$$

$n \geq 1$ leads to finite λ in Eq. (15). However, $n \geq 2$ is necessary for s_h to be finite in Eq. (16). Additionally, experimentally it
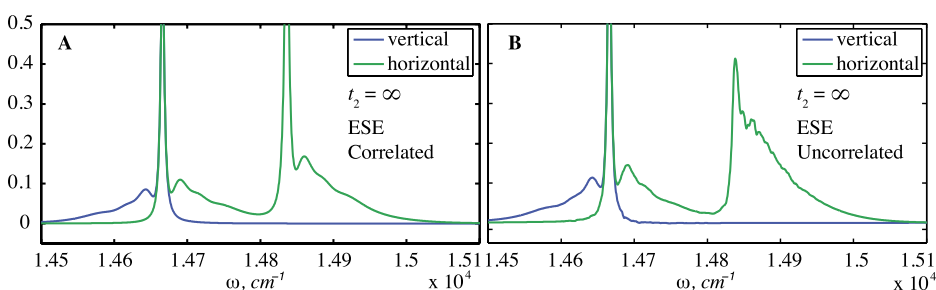
FIG. 11. Vertical and horizontal cross sections at $\omega_1 = 14\,666$ cm^{-1} of the real part (absorptive signal) of ESE of WSCP-inspired dimer at $t_2 = \infty$ (Figure 9). A: modeled with correlated static energy disorder; B: modeled with uncorrelated static energy disorder. Blue—vertical cross section; green—horizontal cross section.

is usually observed that $J(\omega) \to 0$ as $\omega \to 0$[44] what is possible when $n \geq 3$.

The spectral density determines the behavior of the line shape function (Eq. (3)). For example, the response function decays, and the absorption lines of Eq. (5) have finite width if at long times $\Re(g(t)) \to \gamma t$, with γ being some constant. This constant also becomes the width of the ZPL, which is the electronic-only transition. Analytical calculations lead to

$$\gamma = \Re \int_0^\infty dt C(t) = T \lim_{\omega \to 0} \frac{C''(\omega)}{\omega}. \tag{19}$$

For the model of Eq. (17), the linewidth is equal to $T a_n \omega^{n-1}$. So, essentially, the spectral linewidths of all peaks (including the ZPL) become related to the very low frequency part of spectral density. As we requested that $n \geq 3$, we obtain that $\gamma = 0$. This implies that according to the linear-coupling theory, the ZPL is an infinitely narrow Dirac-peak.

Instead of linear growth of $g(t)$ function, we could request $g(t) \to \sigma^2 t^2$. However, taking into account that $\frac{d^2}{dt^2} g(t) = C(t)$, this leads to $2\sigma^2 = C(t = \infty)$, and the correlation function must never decay, which contradicts the finite memory concept. (Unless we assume fractal-like system dynamics; however, simple solutions should not behave like that.) So $g(t) \propto t^n$ with $n > 2$ leads to unphysical growing-up correlation function.

Thus, the linear coupling theory leads to temperature independent zero-width ZPL and the linear system-bath coupling model is insufficient. The quadratic coupling hence becomes necessary to account for this property (i.e., ZPL width). It has been shown that the finite linewidth of the ZPL emerges from the simple quadratic coupling model.[56,57] The latter is also demonstrated for an arbitrary correlation function and by including only the second-order cumulants shown in the Appendix.

Besides the dynamic contribution to the overall stochasticity, the slow-to-static fluctuations, more often referred-to as the conformational or diagonal disorder, introduce additional static energy configuration in space. The average energy landscape defines funnels of the energy and electron transport.[67] The deviations from this mean introduce various irregularities, e.g., traps or detours. For example, such deviations may be the source of the proposed two charge separation pathways in the photosystem II reaction centers.[50,68,69]

Nonlinearity or anharmonicity of the static and dynamic environmental fluctuations has been recently proposed to be evident in the LH2 aggregate.[70] We found that one part of nuclear DOF turns from static into dynamic as the temperature is raised from 77 K to ambient. This denotes the temperature-dependent vibrational frequencies: as the temperature is raised, the frequencies increase. The dependence of the nuclear frequencies on the originating electronic state denotes effectively the same type of nonlinearity. However, now the shift from the equilibrium occurs due to change in the electronic configuration.

When all nuclear DOF are treated as separate modes of the environment of electronic-only subsystem, the phonon as well as the intramolecular degrees of freedom are treated at the same level. However, recently, it has been proposed that specific vibrational high-frequency modes with vibrational frequencies close to electronic or excitonic energy gaps

induce the eigen energy shifts, and the peculiar coupled electronic-vibrational beats in coherent short-time 2DES dynamics.[20,22,23] Clear peaks from the high frequency vibrations are also seen in WSCP in the FLN and HB spectra at cryogenic temperatures.[36,37] We do not consider such modes in our study; however, their anharmonicity and consequently dependence on the electronic state as well as their temperature dependence may be an important factor, which can be addressed in the low-T 2DES measurement. The countable number of nuclear vibrations could be in principle included in the modeling explicitly. The other modes, which are more or less off resonant, can be included through the spectral density. Using such approach, the spectral density should indeed account for the phonon DOF, which contain vibrational frequencies up to few hundred cm^{-1} and create smooth $C''(\omega)$ functional form.

The simplest widely used model of the static disorder is to assume that the energies of the relevant chromophores fluctuate independently. This is in accord with the hypothesis of the independent surrounding for each chromophore. However, if the conformational disorder is not local, then chromophore energy fluctuations should be correlated to some extent. The two limits of these correlations are either fully correlated or anti-correlated. Such mechanisms are easily understood for the electronic origin of the fluctuations. In this case, the mere orientation of the chromophores may determine positive or negative correlation of the site energies. The mechanism could be in place for tightly packed chromophores in LH2 antenna or reaction centers. Comparison of our simulations with experiments points to uncorrelated with a slight degree of anti-correlated fluctuation case.[37]

The 2DES spectra contain a controlled delay time t_2. We have showed that the $t_2 = \infty$ delay time describes the phonon spectral density, as well as disorder, in the same way as HB and FLN spectroscopy (additionally the correlation properties of the disorder can be obtained from the cross-peak elongation directions). However, the $t_2 = 0$ delay, as well as intermediate times, contains important information on spectral density with respect to different electronic transitions. For instance, in Figure 10(b), the horizontal cross section at $t_2 = 0$ shows the ZPL and the PSB, which originate due to the transitions coming from electronic ground state. The nuclear equilibrium, hence, is with respect to the electronic ground state. However, in $t_2 = \infty$, the transitions in ESE configurations originate from electronic excited state. Here, the nuclear equilibrium is with respect to the electronic excited state. In our model, we have the same spectral density and the same PSB in these two cases. However, as noticed above, the ZPL contains non-zero linewidth when the nuclear DOF are not harmonic. Therefore, different spectral densities should be attributable to the transitions originating from the electronic ground state and the transitions originating from the electronic excited state. These are then accessible in 2DES at different delay times.

B. Traces of the nuclear dynamics in 2DES

Revealing both the dynamic and static overall contributions to the energy fluctuations is very important in determining functioning properties of molecular systems. The spectral

profiles of the 2DES signals at few-K temperatures allow to reveal this complex information in a single experiment, and thus, to establish connection with the FLN and HB techniques.

In particular, from 2D spectra, one can now deduce the relationship between the properties of the static disorder from the major peak profiles. Following the ZPP elongation of an arbitrary diagonal peak along the diagonal line, one can determine the statistics of the disorder of this specific electronic (or excitonic) transition, i.e., the energy distribution function of the specific state. This is clear by inspecting Figure 8 at zero t_2 delay, where the properties of the electronic ground state are revealed (notice that effectively the system does not spend any time in the excited state).

Second feature of the static energy disorder is the correlation between electronic (excitonic) states. This information is available from the cross-peaks in Figure 8. The elongation direction of the cross-peak shows this correlation: that is, the elongation along the diagonal shows the positive correlation (in this case, the ZPP remains well resolved), while the elongation across the diagonal corresponds to negative correlation or anti-correlation. Similar elongated line shapes have been obtained when studying dynamic fluctuations of vibrations in 2D infrared spectroscopy.[71] At $t_2 = \infty$, the correlation properties of the relaxed electronic excited states are imprinted in the cross-peak below the diagonal and can be revealed from the ESE contributions (see Figure 9 middle column). Notice that in present simulations, the static disorder has indeed no time scale so the ESE peaks remain elongated along the diagonal.

Of course, the notion of *static* is relative and depends on what time scale is under consideration. The total lifetime of an exciton in a photosynthetic antenna in the absence of traps is on the order of nanoseconds.[65] Thus, the fluctuations, which occur on microsecond time scale, will always show up as static. However, the fluctuations which occur within picoseconds will be reflected in peak shape dynamics as a function of t_2 delay time and may show effective decay of correlation or anti-correlation in off-diagonal peak shapes. However, these fluctuations do not affect the homogeneous line shapes, because the spectral peak is shaped by decay function of the optical response.[55] The corresponding decay time scale is within hundreds of femtoseconds. Thus, the picosecond fluctuations are static with respect to the homogeneous line shape, but they are dynamic with respect to exciton lifetime. Such fluctuations are often referred-to as the spectral diffusion and may be observed in 2DES spectra as a function of t_2.

C. 2DES line shape features related to HB and FLN experiments

As described in Sec. II, the cross sections of the 2DES spectra can be compared with the HB and FLN measurement. Though we model the spectra of an excitonic homodimer coupled to a thermal bath, several parameters were taken from experiment (*vide supra*). Although, as mentioned above, an explicit quantitative comparison with experimental data obtained for tetramer of CaWSCP protein[36,37] cannot be made, a qualitative analysis reveals that many spectral features can be successfully identified (see Figures 10 and 11).

We find that vertical PP cross sections, which compare with transient HB and/or PHB spectra, best represent the experiments in the case of uncorrelated diagonal disorder. In the vertical cross sections (Figure 10), we can in principle distinguish a narrow sharp spectral hole with real and pseudophonon side bands on the higher and lower energy sides, respectively. This feature originates from the vertical cross section of the diagonal peak. Therefore, real and pseudo-PSB reflect shapes of the diagonal peak above and below diagonal, respectively. The origin of these features is the same as in traditional HB. Then, we see rather broad shallow satellite holes, which appear due to excitonic delocalization of the pigment excitation. These originate as the cross sections of the cross-peaks in 2DES. They represent the coupling between different pigments as in HB.

The ESA component of the 2DES produces positive features. It is now a matter of interpretation, whether these features could be called by "anti-holes." It is essentially absorption at different frequency than available before excitation/burning (excitation during t_1 delay). Its energy can be adjusted by means of the bi-exciton binding energy.

This is in contrast with the typical interpretation of the anti-hole origin, especially formed during the NPHB process.[31] In standard NPHB, the anti-hole corresponds to the electronic absorption from the electronic ground state of the bleached pigments that after burning reside in a rearranged immediate environment (i.e., these pigments absorb at different frequencies). However, in our interpretation of 2DES, the whole aggregate after excitation does not return to the electronic ground state (which is reminiscent of transient HB). Therefore, the original absorption is missing (hence, the bleach or hole feature) and the extra absorption (or the anti-hole-like feature) comes from electronic excitation of the whole aggregate to its next (i.e., double) electronic state. Here, one must distinguish the difference between the pigment excitations, and the delocalized exciton states of the aggregate; that is, in the case of pigment aggregates, the optical lasers affect the *exciton states*. In this interpretation, the 2DES post-burn "anti-hole" spectrum corresponds to optical transition from thermalized single-exciton to double-exciton manifolds. When this absorption is in the same spectral region as the original absorption, its explicit position can be tuned by bi-exciton binding energy (electrochromic shift). This approach takes into account that different electronic configurations of one of the chromophores (electronic excited vs electronic ground) affect the excitation energy of the neighboring chromophore.[62]

Additionally, we could obtain the sharp anti-holes on the higher-energy sides of the main hole, by assuming the pigments with three electronic states (i.e., by including overtone states). The satellite holes can be also produced by high frequency intramolecular vibrations. There are no principal obstacles to include these features in the future modeling.

VII. CONCLUSIONS

It has been demonstrated that low-temperature 2DES spectroscopy can reveal the nuclear DOF coupling to elec-

tronic transitions. The profiles of the ZPPs and the PSBs provide a new insight into dynamic, static fluctuational properties, as well as the slow spectral diffusion. Different types of correlations between various electronic states are also observed. Vertical cross section of the 2DES at $t_2 = \infty$ delay time can be correlated with the traditional HB spectroscopy at weak burn fluences. The vertical cross sections of its ESE contribution at this delay time correspond to the FLN spectra. Qualitatively different and novel information is obtained from the spectral line shapes of 2DES at $t_2 = 0$, which reveal the spectral densities with respect to the electronic ground state. The latter is in contrast to FLN approach, where the spectral density is measured with respect to the electronic excited state. Consequently, we propose that low-temperature 2DES data obtained at various t_2 delays could reveal the dynamical relaxation of the spectral density due to the anharmonic nature of the system-bath coupling.

ACKNOWLEDGMENTS

APPENDIX: DERIVATION OF THE ZPL WIDTH PARAMETERS

Consider a chromophore with two electronic states $|g\rangle$ and $|e\rangle$ coupled to a set of harmonic modes. Such a system is described by a Hamiltonian of the displaced unit-mass harmonic multidimensional oscillators, and $\hat{p}_\alpha$, $\hat{q}_\alpha$, and d_α are the momentum operator, coordinate operator, and shift of nuclear mode α, respectively. The linear coupling theory leads to temperature independent zero-width ZPL. It has been shown that the finite linewidth of the ZPL emerges from the simple quadratic coupling model.[56,57] The latter can be simply demonstrated as follows. The system-bath coupling Hamiltonian can be generalized as

$$\hat{H}_{SB} = \Delta(\{\hat{q}_\alpha\})|e\rangle\langle e| \tag{A1}$$

with

$$\Delta(\{q_\alpha\}) = -\sum_\alpha \omega_\alpha d_\alpha \hat{q}_\alpha + \omega_\alpha h_\alpha \hat{q}_\alpha^2. \tag{A2}$$

The linear response function due to photo-induced polarization of the system (disregarding laser polarization)[28,55] is given by

$$R^{(1)}(t) = i\theta(t)\langle \hat{P}G(t)\hat{P}\rho_g \rangle + c.c., \tag{A3}$$

where angular brackets denote the trace over the equilibrium described by the density operator ρ_g, $\hat{P}$ is a polarization operator, $G(t) = \exp(-i\hat{H}t)$ is the time propagator, and $\theta(t)$ is the Heaviside function.

The relevant quantity for the linear response is the propagator of electronic coherence eg traced over the bath,

$$G_{eg}(t) = e^{-i\varepsilon t}\langle F(t)\rangle_B, \tag{A4}$$

where $F(t)$ is the bath-related dephasing operator. This trace can be approximately expanded using the second order cumulants provided $h_\alpha \ll d_\alpha$. Taking the system-bath coupling parameter from Eq. (A2) as $\Delta(\{q_\alpha\}) \equiv A + B$, we calculate the bath-related dephasing operator of Eq. (A4),

$$\langle F(t)\rangle_B = \left\langle \exp_T\left(-i\int_0^t d\tau \Delta(\tau)\right)\right\rangle_B. \tag{A5}$$

For that, we use a cumulant expansion[72]

$$\langle F(t)\rangle_B = \exp\left(\sum_{n=1}^\infty K_n(t)\right), \tag{A6}$$

where the expansion terms are

$$K_n(t) = (-i)^n \int_0^t dt_n \ldots \int_0^{t_2} dt_1 \langle \Delta(t_n)\Delta(t_{n-1})\ldots\Delta(t_1)\rangle_c. \tag{A7}$$

For simplicity, assuming that the quadratic coupling is much smaller than the linear one and its strength in energy scale is much smaller than the thermal energy, we truncate the expansion at the second order. The first order cumulant is given by

$$\langle \Delta(t_1)\rangle_c = \langle \Delta(t_1)\rangle = \langle B\rangle = \sum_\alpha \omega_\alpha h_\alpha z_\alpha, \tag{A8}$$

where $z_\alpha = \coth(\beta\omega_\alpha/2)/2$. The second order cumulant is slightly more complicated,

$$\langle \Delta(t_2)\Delta(t_1)\rangle_c = \langle \Delta(t_2)\Delta(t_1)\rangle - \langle \Delta(t_2)\rangle\langle \Delta(t_1)\rangle \tag{A9}$$

$$= \langle A(t_2)A(t_1)\rangle + \langle B(t_2)B(t_1)\rangle - \langle B\rangle^2. \tag{A10}$$

For the first term, we have

$$\langle A(t_2)A(t_1)\rangle = C(t_2 - t_1), \tag{A11}$$

which is a regular fluctuation-correlation function coming from the linear-coupling term. The next term,

$$\langle B(t_2)B(t_1)\rangle = \sum_\alpha \omega_\alpha^2 h_\alpha^2 \langle \hat{q}_\alpha(t_2)\hat{q}_\alpha(t_2)\hat{q}_\alpha(t_1)\hat{q}_\alpha(t_1)\rangle. \tag{A12}$$

Wick's theorem dictates that

$$\langle \hat{q}_\alpha(t_2)\hat{q}_\alpha(t_2)\hat{q}_\alpha(t_1)\hat{q}_\alpha(t_1)\rangle = \langle \hat{q}_\alpha(t_2)\hat{q}_\alpha(t_2)\rangle\langle \hat{q}_\alpha(t_1)\hat{q}_\alpha(t_1)\rangle$$
$$+ 2\langle \hat{q}_\alpha(t_2)\hat{q}_\alpha(t_1)\rangle\langle \hat{q}_\alpha(t_2)\hat{q}_\alpha(t_1)\rangle, \tag{A13}$$

leading to

$$\langle B(t_2)B(t_1)\rangle = \sum_\alpha \omega_\alpha^2 h_\alpha^2 \left(z_\alpha^2 + 2\left(\langle \hat{q}_\alpha(t_2)\hat{q}_\alpha(t_1)\rangle\right)^2\right). \tag{A14}$$

We can denote

$$\mathcal{B}(t) = \sum_\alpha \frac{\omega_\alpha^2 h_\alpha^2}{4}(\cos(\omega_\alpha t)\coth(\beta\omega_\alpha/2) - i\sin(\omega_\alpha t))^2. \tag{A15}$$

So

$$\langle \Delta(t_2)\Delta(t_1)\rangle_c = C(t_2 - t_1) + \mathcal{B}(0) + 2\mathcal{B}(t_2 - t_1) - \langle B\rangle^2. \tag{A16}$$

Using these two cumulants, the response function can be given in the same functional form as for the linear system-bath

coupling model[28,55] while the spectral line shape function is given by

$$g(t) = \langle B \rangle \cdot t + \left(\mathcal{B}(0) - \langle B \rangle^2 \right) \frac{t^2}{2} + \int_0^t d\tau_2 \int_0^{\tau_2} d\tau_1 \left(C(t_2 - t_1) + 2\mathcal{B}(t_2 - t_1) \right). \tag{A17}$$

Additionally, in the integral, we can use that $C(t_2 - t_1) \gg \mathcal{B}(t_2 - t_1)$, so $\mathcal{B}(t)$ function can be neglected. Thus, the spectral line shape function becomes

$$g(t) \approx \bar{\gamma} t + \bar{\sigma}^{(2)} \frac{t^2}{2} + g_l(t),$$

where

$$\bar{\gamma} = \sum_\alpha \frac{\omega_\alpha h_\alpha}{2} \coth(\beta \omega_\alpha / 2) \tag{A18}$$

and

$$\bar{\sigma}^{(2)} = - \sum_{\alpha \alpha'}^{\alpha \neq \alpha'} \frac{\omega_\alpha h_\alpha \omega_{\alpha'} h_{\alpha'}}{4} \coth(\beta \omega_\alpha / 2) \coth(\beta \omega_{\alpha'} / 2) \tag{A19}$$

are real-valued temperature-dependent constants while $g_l(t)$ is the line shape function of the linear coupling model. These complicated expressions could be evaluated for the specific model of vibrational modes of the molecule. However, we have to request that $\bar{\gamma} \geq 0$ and $\bar{\sigma} \geq 0$. This is possible when h_α has some alternating character for different modes so that the product $h_\alpha h_{\alpha'}$ for $\alpha \neq \alpha'$ is negative number.

We thus obtain that the quadratic coupling creates additional line broadening.[56,57] It can cause Lorentzian (when $\bar{\gamma} > \bar{\sigma}$) or Gaussian (when $\bar{\gamma} < \bar{\sigma}$) line shapes.

[1]G. Engel, T. Calhoun, E. Read, T. Ahn, T. Mančal, Y.-C. Cheng, R. Blankenship, and G. Fleming, Nature **446**, 782 (2007).

[2]A. F. Fidler, V. P. Singh, P. D. Long, P. D. Dahlberg, and G. S. Engel, J. Chem. Phys. **139**, 155101 (2013).

[3]J. Dostál, T. Mančal, R. Augulis, F. Vácha, J. Pšenčik, and D. Zigmantas, J. Am. Chem. Soc. **134**, 11611 (2012).

[4]D. Abramavicius, B. Palmieri, D. V. Voronine, F. Šanda, and S. Mukamel, Chem. Rev. **109**, 2350 (2009).

[5]F. D. Fuller, J. Pan, A. Gelzinis, V. Butkus, S. S. Senlik, D. E. Wilcox, C. F. Yocum, L. Valkunas, D. Abramavicius, and J. P. Ogilvie, Nat. Chem. **6**, 706 (2014).

[6]S. Mukamel, Annu. Rev. Phys. Chem. **51**, 691 (2000).

[7]E. Romero, R. Augulis, V. I. Novoderezhkin, M. Ferretti, J. Thieme, D. Zigmantas, and R. van Grondelle, Nat. Phys. **10**, 676 (2014).

[8]G. S. Schlau-Cohen, T. R. Calhoun, N. S. Ginsberg, E. L. Read, M. Ballottari, R. Bassi, R. van Grondelle, and G. R. Fleming, J. Phys. Chem. B **113**, 15352 (2009).

[9]E. Collini and G. D. Scholes, Science **323**, 369 (2009).

[10]F. Milota, J. Sperling, A. Nemeth, and H. Kauffmann, Chem. Phys. **357**, 45 (2009).

[11]T. Brixner, J. Stenger, H. M. Vaswani, M. Cho, R. E. Blankenship, and G. R. Fleming, Nature **434**, 625 (2005).

[12]T. Mančal, L. Valkunas, E. L. Read, G. S. Engel, T. R. Calhoun, and G. R. Fleming, Spectroscopy **22**, 199 (2008).

[13]G. Panitchayangkoon, D. Hayes, K. A. Fransted, J. Caram, E. Harel, J. Wen, R. Blankenship, and G. Engel, Proc. Natl. Acad. Sci. U. S. A. **107**, 12766 (2010).

[14]G. Panitchayangkoon, D. V. Voronine, D. Abramavicius, J. R. Caram, N. H. C. Lewis, S. Mukamel, and G. S. Engel, Proc. Natl. Acad. Sci. U. S. A. **108**, 20908 (2011).

[15]E. Harel and G. S. Engel, Proc. Natl. Acad. Sci. U. S. A. **109**, 706 (2012).

[16]M. Ferretti, V. I. Novoderezhkin, E. Romero, R. Augulis, A. Pandit, D. Zigmantas, and R. van Grondelle, Phys. Chem. Chem. Phys. **16**, 9930 (2014).

[17]N. Christensson, F. Milota, J. Hauer, J. Sperling, O. Bixner, A. Nemeth, and H. Kauffmann, J. Phys. Chem. B **115**, 5383 (2011).

[18]S. Westenhoff, D. Paleček, P. Edlund, P. Smith, and D. Zigmantas, J. Am. Chem. Soc. **134**, 16484 (2012).

[19]G. D. Scholes, G. R. Fleming, A. Olaya-Castro, and R. van Grondelle, Nature Chem. **3**, 763 (2011).

[20]V. Butkus, L. Valkunas, and D. Abramavicius, J. Chem. Phys. **140**, 034306 (2014).

[21]A. W. Chin, J. Prior, R. Rosenbach, F. Caycedo-Soler, S. F. Huelga, and M. B. Plenio, Nat. Phys. **9**, 113 (2013).

[22]V. Butkus, D. Zigmantas, L. Valkunas, and D. Abramavicius, Chem. Phys. Lett. **545**, 40 (2012).

[23]V. Butkus, D. Zigmantas, D. Abramavicius, and L. Valkunas, Chem. Phys. Lett. **587**, 93 (2013).

[24]V. Butkus, L. Valkunas, and D. Abramavicius, J. Chem. Phys. **137**, 044513 (2012).

[25]D. Egorova, J. Chem. Phys. **140**, 034314 (2014).

[26]D. Abramavicius and L. Valkunas, Photosynth. Res. **2015**, 1.

[27]V. May and O. Kühn, *Charge and Energy Transfer Dynamics in Molecular Systems* (Wiley-VCH Verlag GmbH & Co. KGaA, Weinheim, Germany, 2011), p. 562.

[28]L. Valkunas, D. Abramavicius, and T. Mančal, *Molecular Excitation Dynamics and Relaxation* (Wiley-VCH Verlag GmbH & Co. KGaA, Weinheim, Germany, 2013).

[29]A. Ishizaki and G. R. Fleming, J. Chem. Phys. **130**, 234111 (2009).

[30]V. Novoderezhkin, J. Dekker, H. van Amerongen, and R. van Grondelle, Biophys. J. **93**, 1293 (2007).

[31]R. Jankowiak, M. Reppert, V. Zazubovich, J. Pieper, and T. Reinot, Chem. Rev. **111**, 4546 (2011).

[32]M. Rätsep and A. Freiberg, J. Lumin. **127**, 251 (2007).

[33]M. Rätsep, J. Pieper, K.-D. Irrgang, and A. Freiberg, J. Phys. Chem. B **112**, 110 (2008).

[34]T. Renger and R. A. Marcus, J. Chem. Phys. **116**, 9997 (2002).

[35]M. Rätsep, J. Linnanto, and A. Freiberg, J. Chem. Phys. **130**, 194501 (2009).

[36]J. Pieper, M. Rätsep, I. Trostmann, G. Renger, and A. Freiberg, J. Phys. Chem. B **115**, 4042 (2011).

[37]J. Pieper, M. Rätsep, I. Trostmann, F.-J. Schmitt, C. Theiss, H. Paulsen, H. Eichler, A. Freiberg, and G. Renger, J. Phys. Chem. B **115**, 4053 (2011).

[38]J. Pieper, M. Rätsep, K.-D. Irrgang, and A. Freiberg, J. Phys. Chem. B **113**, 10870 (2009).

[39]D. Abramavicius, V. Butkus, J. Bujokas, and L. Valkunas, Chem. Phys. **372**, 22 (2010).

[40]J. Han, H. Zhang, and D. Abramavicius, J. Chem. Phys. **139**, 034313 (2013).

[41]T. Renger, M. E. Madjet, F. Muh, I. Trostmann, F.-J. Schmitt, C. Theiss, H. Paulsen, H. J. Eichler, A. Knorr, and G. Renger, J. Phys. Chem. B **113**, 9948 (2009).

[42]D. Bednarczyk, S. Takahashi, H. Satoh, and D. Noy, Biochim. Biophys. Acta, Bioenerg. **1847**, 307 (2015).

[43]J. Alster, H. Lokstein, J. Dostál, A. Uchida, and D. Zigmantas, J. Phys. Chem. B **118**, 3524 (2014).

[44]A. Kell, X. Feng, M. Reppert, and R. Jankowiak, J. Phys. Chem. B **117**, 7317 (2013).

[45]V. Butkus, D. Abramavicius, A. Gelzinis, and L. Valkunas, Lith. J. Phys. **50**, 267 (2010).

[46]W. M. Zhang, T. Meier, V. Chernyak, and S. Mukamel, J. Chem. Phys. **108**, 7763 (1998).

[47]D. Abramavicius, L. Valkunas, and S. Mukamel, Europhys. Lett. **80**, 17005 (2007).

[48]D. Abramavicius, D. V. Voronine, and S. Mukamel, Biophys. J. **94**, 3613 (2008).

[49]F. Milota, J. Sperling, A. Nemeth, D. Abramavicius, S. Mukamel, and H. F. Kauffmann, J. Chem. Phys. **131**, 054510 (2009).

[50]R. Jankowiak, J. Phys. Chem. Lett. **3**, 1684 (2012).

[51]S. Völker, Annu. Rev. Phys. Chem. **40**, 499 (1989).

[52]V. Zazubovich, J. Phys. Chem. B **118**, 13535 (2014).

[53]R. Jankowiak, J. M. Hayes, and G. J. Small, Chem. Rev. **93**, 1471 (1993).

[54]M. Reppert, V. Naibo, and R. Jankowiak, J. Chem. Phys. **133**, 014506 (2010).

[55]S. Mukamel, *Principles of Nonlinear Optical Spectroscopy* (Oxford University Press, New York, 1995).

[56]D. Hsu and J. L. Skinner, J. Chem. Phys. **81**, 1604 (1984).

[57]J. L. Skinner and D. Hsu, J. Phys. Chem. **90**, 4931 (1986).

[58]T. Meier, V. Chernyak, and S. Mukamel, J. Chem. Phys. **107**, 8759 (1997).

[59]T. Reinot, V. Zazubovich, J. M. Hayes, and G. J. Small, J. Phys. Chem. B **105**, 5083 (2001).

[60]M. Rätsep, M. Pajusalu, and A. Freiberg, Chem. Phys. Lett. **479**, 140 (2009).

[61]J. L. Hughes, R. Razeghifard, M. Logue, A. Oakley, T. Wydrzynski, and E. Krausz, J. Am. Chem. Soc. **128**, 3649 (2006).

[62]D. Abramavicius, B. Palmieri, and S. Mukamel, Chem. Phys. **357**, 79 (2009).

[63]M. Yang and G. R. Fleming, Chem. Phys. **282**, 163 (2002).

[64]Y. Tanimura, J. Phys. Soc. Jpn. **75**, 082001 (2006).

[65]H. van Amerongen, L. Valkunas, and R. van Grondelle, *Photosynthetic Excitons* (World Scientific, Singapore, New Jersey, London, Hong Kong, 2006), p. 590.

[66]A. Gall, A. A. Pascal, and B. Robert, Biochim. Biophys. Acta, Bioenerg. **1847**, 12 (2015).

[67]D. Abramavicius and S. Mukamel, J. Phys. Chem. B **113**, 6097 (2009).

[68]V. I. Novoderezhkin, E. Romero, J. P. Dekker, and R. van Grondelle, ChemPhysChem **12**, 681 (2011).

[69]A. Gelzinis, L. Valkunas, F. D. Fuller, J. P. Ogilvie, S. Mukamel, and D. Abramavicius, New J. Phys. **15**, 075013 (2013).

[70]O. Rancova and D. Abramavicius, J. Phys. Chem. B **118**, 7533 (2014).

[71]R. Venkatramani and S. Mukamel, J. Chem. Phys. **117**, 11089 (2002).

[72]R. Kubo, J. Phys. Soc. Jpn. **17**, 1100 (1962).

[73]A. Kell *et al.*, unpublished data (2015).